ANALYTICAL SOLUTION FOR THE PROPAGATION OF FINITE CRESTED LONG WAVES OVER A SLOPING BEACH

A THESIS SUBMITTED TO
THE GRADUATE SCHOOL OF NATURAL AND APPLIED SCIENCES
OF
MIDDLE EAST TECHNICAL UNIVERSITY

BY

AHMED SABRİ YAĞMUR

IN PARTIAL FULFILLMENT OF THE REQUIREMENTS
FOR
THE DEGREE OF MASTER OF SCIENCE
IN
AEROSPACE ENGINEERING

FEBRUARY 2022

Approval of the thesis:

ANALYTICAL SOLUTION FOR THE PROPAGATION OF FINITE CRESTED LONG WAVES OVER A SLOPING BEACH

submitted by **AHMED SABRİ YAĞMUR** in partial fulfillment of the requirements for the degree of **Master of Science in Aerospace Engineering Department, Middle East Technical University** by,

Prof. Dr. Halil Kalıpçılar
Dean, Graduate School of **Natural and Applied Sciences** _____

Prof. Dr. Serkan Özgen
Head of Department, **Aerospace Engineering** _____

Assoc. Prof. Dr. Utku Kânoğlu
Supervisor, **Department of Engineering Sciences, METU** _____

Examining Committee Members:

Prof. Dr. Yusuf Özyörük
Department of Aerospace Engineering, METU _____

Assoc. Prof. Dr. Utku Kânoğlu
Department of Engineering Sciences, METU _____

Prof. Dr. Ünver Kaynak
Department of Aerospace Engineering, AYBU _____

Prof. Dr. Hakan I. Tarman
Department of Mechanical Engineering, METU _____

Assist. Prof. Dr. Baran Aydın
Department of Civil Engineering, ATU _____

Date: 10.02.2022

I hereby declare that all information in this document has been obtained and presented in accordance with academic rules and ethical conduct. I also declare that, as required by these rules and conduct, I have fully cited and referenced all material and results that are not original to this work.

Name, Surname: Ahmed Sabri Yağmur

Signature :

ABSTRACT

ANALYTICAL SOLUTION FOR THE PROPAGATION OF FINITE CRESTED LONG WAVES OVER A SLOPING BEACH

Yağmur, Ahmed Sabri
M.S., Department of Aerospace Engineering
Supervisor: Assoc. Prof. Dr. Utku Kânoğlu

February 2022, 58 pages

The analytical solution of shallow water-wave equations, both linear and nonlinear, is widely used to provide an insightful understanding of the coastal effect of long waves. These solutions are generally carried out for two-dimensional (1 space + 1 time) propagation, even though there are a limited number of analytical solutions for the three-dimensional (2 space + 1 time) propagation. Three-dimensional propagation of long waves over a sloping beach is considered here. The analytical solution is obtained using the linear shallow water-wave theory resulting in double indefinite integrals. The solution is evaluated using various numerical methods, and results are discussed.

Keywords: analytical solution, shallow water, long waves, finite crest, tsunami

ÖZ

SONLU KRET UZUNLUĞUNA SAHİP UZUN DALGALARIN EĞİMLİ KIYI ÜZERİNDEKİ YAYILIMININ ANALİTİK ÇÖZÜMÜ

Yağmur, Ahmed Sabri
Yüksek Lisans, Havacılık ve Uzay Mühendisliği Bölümü
Tez Yöneticisi: Doç. Dr. Utku Kânoğlu

Şubat 2022 , 58 sayfa

Hem doğrusal hem de doğrusal olmayan sığ su dalgası denklemlerinin analitik çözümleri, uzun dalgaların kıyı etkilerini anlamak için yaygın olarak kullanılmaktadır. Bu çözümler genellikle iki-boyutlu (1 uzay + 1 zaman) yayılım için mevcut olsa da sınırlı sayıda üç-boyutlu (2 uzay + 1 zaman) yayılıma ait çözümler de vardır. Bu araştırmada, eğimli bir kıyı üzerinde uzun dalgaların üç-boyutlu yayılımı ele alınmaktadır. Analitik çözüm, doğrusal sığ su dalga teorisi kullanılarak çift sonsuz integraller olarak elde edilmiştir. Çözüm çeşitli yöntemler kullanılarak hesaplanmış ve sonuçlar tartışılmıştır.

Anahtar Kelimeler: analitik çözüm, sığ su, uzun dalgalar, sonlu kret, tsunami

To my family, teachers, and friends

ACKNOWLEDGMENTS

I would like to thank Assoc. Prof. Utku Kânoğlu for his constant supervision throughout the process of writing this thesis, and to Asst. Prof. Dr. Baran Aydın for his contributions, guidance and constant help.

I am especially indebted to Prof. Dr. Hakan I. Tarman for his invaluable contributions regarding the numerical evaluation of the integrals, and am grateful to Dr. Güven Yücesan for the fruitful discussions I had with him regarding the same matter. I appreciate the help provided by Dr. Mehmet Karaca regarding coding in Fortran.

I would also like to thank Prof. Dr. Yusuf Özyörük and Prof. Dr. Ünver Kaynak for their valued suggestions.

The process of researching and writing a thesis is an arduous one, and I would like to express my heartfelt gratitude to my parents, Fatma and Yalçın Yağmur, for their constant love and support.

Lastly, I would like to acknowledge the support by The Scientific and Technological Research Council of Turkey (TÜBİTAK) through project number 119Y014.

TABLE OF CONTENTS

LIST OF TABLES

TABLES

LIST OF FIGURES

FIGURES

CHAPTER 1

INTRODUCTION

Tsunamis are surface gravity waves generated by impulsive geophysical events forcing the seafloor or coastal topography. Different mechanisms can generate tsunamis. Of these, the most common is underwater earthquakes. Other mechanisms include underwater landslides and collapses, underwater volcanic eruptions, sharp changes in atmospheric pressure. The possibility of tsunamis originating from falling meteorites is also worth mentioning (Levin, Nosov, et al., 2009).

Tsunamis propagate long distances, i.e., across the oceans, as a series of waves. Tsunamis are known to have wavelengths, λ, that are much greater than the depth of the sea over which they propagate. Therefore, they are referred to as long waves as well. The tsunami source is generally characterized by its horizontal dimension, i.e., its wavelength is generally around the order of a hundred kilometers ($\lambda \sim 100$km). Since the average depth, H of the oceans is around 4km; it follows that the wavelength is much greater than the depth ($\lambda \gg H$), justifying the long wave assumption. Periods of tsunamis, i.e., the difference between the arrival time of the highest peak and the next one, range between $10^2 - 10^4$ seconds. In the open ocean, tsunami waves have quite small amplitude. Their amplitudes are rarely greater than 1m across an ocean, even if the displacement amplitude at the source may be of the order of 10m. The relatively small size of the amplitude, coupled with the long period, makes them unnoticeable in the open ocean. However, as the waves approach the coast, the wave amplitude increases. This occurs because a decrease in the water depth leads to a decrease in the propagation velocity of the waves, which leads to the compression of the wave packet. This phenomenon is known as shoaling.

There are many known and recorded tsunami events and they occur most frequently in the Pacific Ocean (Levin, Nosov, et al., 2009). The disastrous near- and far-field effects became more widely recognized after the 2004 Boxing Day tsunami (Kânoğlu et al., 2013). This tsunami was caused by an earthquake of magnitude $M_w = 9.3$ that occurred in the Indian Ocean, near the island of Sumatra. This earthquake was so massive that the waves generated traveled all over the World Ocean. In the regions close to the source, the tsunami runup reached up to 35 m. This catastrophic event led to the death of more than 250,000 people, making it the highest casualty count among all known tsunami events (Levin, Nosov, et al., 2009).

Another noteworthy and peculiar tsunami is the 17 July 2006 Java tsunami. This event was caused by an earthquake of magnitude $M_w = 7.8$ off the south coast of Western Java, Indonesia. Though this earthquake magnitude was not quite as large, unexpectedly large runup values were reached. An impressive runup of 20 m was measured at Permisan. Though there have been different explanations regarding this unexpectedly large runup value, Kânoğlu et al. (2013) showed that Permisan is close to a focusing point and that classic field theory suffices in explaining this "unexpected" value (Kânoğlu et al., 2013).

Japan is known for its earthquakes and tsunamis due to its location being near the subduction zone formed by the Pacific, North America, Philippines and Eurasian plates. The Tohoku-Oki earthquake had a magnitude of $M_w = 9.0$ (as updated), the greatest known magnitude in the history of Japan. The waves generated by this earthquake were enormous. Although the coastal regions had an extensive network of tsunami walls, these walls were not designed to stop waves with runup heights greater than $10 - 15$ m. Since Japan has an extensive monitoring system, quick action could be taken. Also, since the waves slow down as the water depth decreases (i.e., as it approaches the coast), people were able to take quick action. However, some citizens did not evacuate their homes because they believed that the tsunami walls would shield them. Furthermore, erroneous prediction of runup values along the coast of

the Miyagi, Iwate and Fukushima prefectures prevented necessary action from being taken. The real waves overtopped the tsunami walls and damaged the cooling system of the nuclear plant located at Fukishima. This led to explosions and radioctive leakage. Overall, this event led to the deaths of roughly 15,000 people (Gupta and Gahalaut, 2013).

A tsunami propagating along a plane beach, whether it be generated due to earthquakes or landslides, can reach maximum runup values that can be predicted by the two-dimensional (1-space + 1-time) model correct in order of magnitude. However, there are special effects that might increase runup substantially. One of the counter-intuitive phenomena, though previously known, was first studied in depth by Kânoğlu et al. (2013) for tsunamis propagating in a constant depth basin, using the three-dimensional (2-space + 1-time) linearized shallow water-wave equations. In that paper, they determined that finite crested long waves with a dipolar initial profile (N-wave) experience focusing; that is, the water at the transverse edges of the wave break and move towards the bisector line of the depression side. This leads to constructive interference, hence "unexpected" runup values. While propagation over a constant depth basin provides insight into the physics, a more realistic case would be the solution of the two-spatial+one-temporal linearized shallow water-wave equation propagating along a plane beach.

Even though Fujima, Dozono, and Shigemura (2000) solved this problem, they did not perform any analysis regarding focusing phenomena. Instead, they focused on the effects of source directivity, edge wave propagation, and the effect of Coriolis forces. Sammarco and Renzi (2008) studied landslide tsunamis propagating along a plane beach. However, they did not discuss anything about focusing either. Renzi and Sammarco (2010) later on, studied landslide tsunamis propagating around a conical island and mentioned that tsunamis generated by similar landslide characteristics reach relatively smaller runup values when propagating around a conical island than when propagating along a plane beach. This is because when long waves propagate along a plane beach, all the edge-wave energy is trapped along the shoreline, whereas in the case of a conical island the energy also propagates in the offshore direction.

Here, the aim is to study the propagation of an earthquake-generated tsunami propagating along a plane beach. The initial waveform is taken as a dipolar profile (N-wave) as proposed by Tadepalli and Synolakis (1994). This profile is very similar to that caused by a seismic fault dislocation by subduction earthquakes (Carrier, Wu, and Yeh, 2003). It is proposed that the unusual runup values can be explained through focusing when the three-dimensional (2-space + 1-time) linear-nondispersive theory is employed. The shoaling phenomenon occurring close to the shoreline cannot be accurately predicted by the linear theory, however, since the main purpose is to observe whether focusing takes place or not, this shortcoming can be disregarded.

(a)

(b)

Figure 1.1: Pictures related to the 2004 tsunami [Retrieved from `https://www.ngdc.noaa.gov`]. (a) View from floor of Triton Hotel, Sri Lanka at 10:11. (b) A flooded village near the coast of Sumatra.

(a)

(b)

Figure 1.2: Pictures showing the effects of the 2011 tsunami [Retrieved from `https://www.ngdc.noaa.gov`]. (a) Flooding near Soma, Fukushima. (b) A Japanese home adrift in the Pacific, near Sendai, Japan.

CHAPTER 2

GOVERNING EQUATIONS

In this chapter, first, derivation of the nonlinear shallow water-wave equations will be presented for a water basin with a depth $h(x, y)$, where x and y denote the horizontal dimensions (Figure 2.1). The nonlinear system will then be linearized. Further, linear system of equations will be reduced to a single hyperbolic differential equation for the wave height, η, denoting perturbation from mean depth h, for wave propagation over a sloping beach. Finally, an analytical solution for the resulting hyperbolic differential equation will be presented.

2.1 The Nonlinear Shallow Water-wave Equations

The nonlinear shallow water-wave equations are derived from the incompressible, inviscid forms of the continuity and momentum equations (Buhler and Helfrich, 2010). The origin is located on the undisturbed free water surface. The velocity vector of the fluid particles is defined as $\vec{U} = u\hat{i} + v\hat{j} + w\hat{k}$, the pressure as p, the bottom topography measured from the free surface as $h(x, y)$, the undisturbed free-surface elevation from undisturbed water level as $\eta(x, y, t)$, and the gravitational acceleration as g. Hence, the governing continuity and momentum equations are given as

$$\vec{\nabla} \cdot \vec{U} = 0, \tag{2.1a}$$

$$\frac{D\vec{U}}{Dt} = -\frac{1}{\rho}\vec{\nabla}p - g\hat{k}, \tag{2.1b}$$

respectively. Here, D/Dt denotes the material derivative.

The pressure at the free surface is atmospheric. However, it is taken as the reference

value for pressure for convenience and hence equals zero. The material derivative of the water surface elevation, $D\eta/Dt$, equals the vertical velocity component at $z = \eta$. The bottom topography is solid; hence no fluid can flow through it, necessitating that the velocity normal to boundary be zero. Therefore, the boundary conditions at the free surface and bottom surface, respectively, are

$$p = 0, \quad \frac{D\eta}{Dt} = \frac{\partial \eta}{\partial t} + \vec{U} \cdot \vec{\nabla}\eta = w, \quad \text{on } z = \eta, \tag{2.2a}$$

$$\vec{U} \cdot \vec{\nabla}[z + h(x, y)] = 0, \quad \text{on } z = -h(x, y). \tag{2.2b}$$

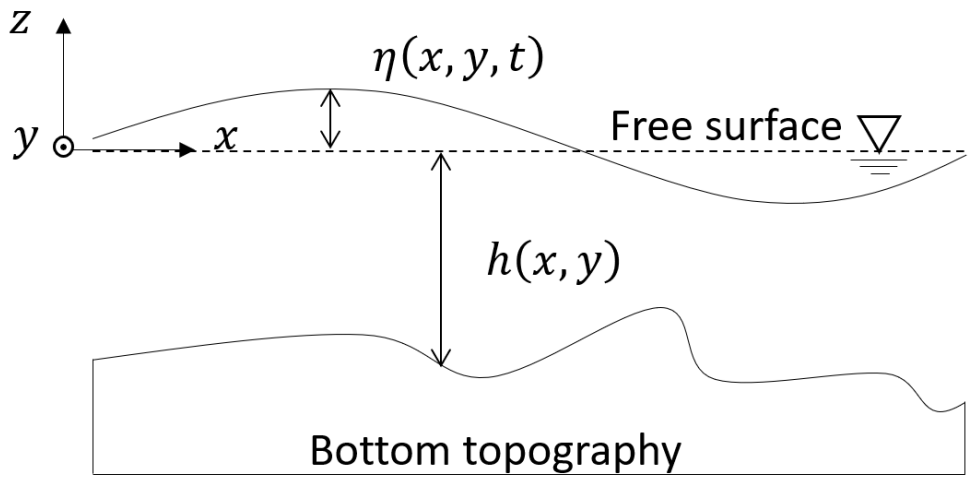

Figure 2.1: Definition sketch.

The aim is to obtain a system of differential equations that inherently contain the boundary conditions given in Equations 2.2a and 2.2b. Therefore, first, the z-component of the momentum equation,

$$\frac{Dw}{Dt} = -\frac{1}{\rho}\frac{\partial p}{\partial z} - g, \tag{2.3}$$

is used to derive an expression for the pressure. The waves' wavelength is relatively large compared with the depth, i.e., the horizontal length scale is much larger than the vertical scale. Therefore, the total change in the vertical velocity of a fluid element with respect to time (Dw/Dt) is negligible compared to the gravitational acceleration and the pressure gradient; thus, it can be neglected, resulting in

$$0 = -\frac{1}{\rho}\frac{\partial p}{\partial z} - g, \tag{2.4}$$

which indicates that the pressure is hydrostatic. Integration of Equation 2.4 from the basin bottom to the free water surface leads to

$$\int_{-h}^{\eta} \frac{\partial p}{\partial z} dz = -\int_{-h}^{\eta} \rho g dz. \tag{2.5}$$

Assuming water is incompressible and neglecting temperature change justify taking constant density. The gravitational acceleration can be assumed to be constant as well, resulting in

$$p(x, y, \eta, t) - p(x, y, z, t) = -\rho g(\eta - z). \tag{2.6}$$

This simplifies to

$$p(x, y, z, t) = \rho g(\eta - z), \tag{2.7}$$

due to the free-surface pressure condition, $p = 0$.

First, the continuity equation is integrated in the z-direction, from the bottom of the sea (basin) to the free surface, i.e.,

$$\int_{-h}^{\eta} \left[\frac{\partial u}{\partial x} + \frac{\partial v}{\partial y} + \frac{\partial w}{\partial z} \right] dz = 0. \tag{2.8}$$

While the Leibniz rule is used to evaluate the first two integrals, the last integrals lead simply to w. Hence, the above integral becomes

$$0 = \frac{\partial}{\partial x} \int_{-h}^{\eta} u dz - u|_{z=\eta} \frac{\partial \eta}{\partial x} + u|_{z=-h} \frac{\partial(-h)}{\partial x} \tag{2.9}$$

$$+ \frac{\partial}{\partial y} \int_{-h}^{\eta} v dz - v|_{z=\eta} \frac{\partial \eta}{\partial y} + v|_{z=-h} \frac{\partial(-h)}{\partial y} \tag{2.10}$$

$$+ w|_{z=\eta} - w|_{z=-h}\,. \tag{2.11}$$

Using the boundary conditions in Equations 2.2a and 2.2b, this simplifies to

$$\frac{\partial \eta}{\partial t} + \frac{\partial}{\partial x} \int_{-h}^{\eta} u dz + \frac{\partial}{\partial y} \int_{-h}^{\eta} v dz = 0. \tag{2.12}$$

Then, using the assumption that the horizontal velocities (u and v) are taken as constant along the depth of the water column, Equation 2.12 becomes

$$\frac{\partial \eta}{\partial t} + \frac{\partial}{\partial x}[u(\eta + h)] + \frac{\partial}{\partial y}[v(\eta + h)] = 0. \tag{2.13}$$

With the above assumptions under consideration, the x- and y-momentum equations become

$$\frac{\partial u}{\partial t} + u\frac{\partial u}{\partial x} + v\frac{\partial u}{\partial y} = -\frac{1}{\rho}\frac{\partial p}{\partial x}, \tag{2.14a}$$

$$\frac{\partial v}{\partial t} + u\frac{\partial v}{\partial x} + v\frac{\partial v}{\partial y} = -\frac{1}{\rho}\frac{\partial p}{\partial y}. \tag{2.14b}$$

Replacing p with the expression in Equation 2.7 results in

$$\frac{\partial u}{\partial t} + u\frac{\partial u}{\partial x} + v\frac{\partial u}{\partial y} + g\frac{\partial \eta}{\partial x} = 0, \tag{2.15a}$$

$$\frac{\partial v}{\partial t} + u\frac{\partial v}{\partial x} + v\frac{\partial v}{\partial y} + g\frac{\partial \eta}{\partial y} = 0. \tag{2.15b}$$

Hence, the following system of partial differential equations (Equations 2.13, 2.15a, 2.15b) are obtained

$$\frac{\partial \eta}{\partial t} + \frac{\partial}{\partial x}[u(\eta + h)] + \frac{\partial}{\partial y}[v(\eta + h)] = 0, \tag{2.16a}$$

$$\frac{\partial u}{\partial t} + u\frac{\partial u}{\partial x} + v\frac{\partial u}{\partial y} + g\frac{\partial \eta}{\partial x} = 0, \tag{2.16b}$$

$$\frac{\partial v}{\partial t} + u\frac{\partial v}{\partial x} + v\frac{\partial v}{\partial y} + g\frac{\partial \eta}{\partial y} = 0, \tag{2.16c}$$

and they are called the nonlinear shallow water-wave equations.

2.2 The Linear Shallow Water-wave Equations

Linearization of the nonlinear shallow water-wave equations is carried out neglecting nonlinear terms to get

$$\frac{\partial \eta}{\partial t} + \frac{\partial (hu)}{\partial x} + \frac{\partial (hv)}{\partial y} = 0, \tag{2.17a}$$

$$\frac{\partial u}{\partial t} + g\frac{\partial \eta}{\partial x} = 0, \tag{2.17b}$$

$$\frac{\partial v}{\partial t} + g\frac{\partial \eta}{\partial y} = 0. \tag{2.17c}$$

Taking t, x, and y derivatives of Equations 2.17a, 2.17b and 2.17c, respectively, and eliminating u and v among these three equations leads to

$$\frac{\partial^2 \eta}{\partial t^2} - g\frac{\partial}{\partial x}\left(h\frac{\partial \eta}{\partial x}\right) - g\frac{\partial}{\partial y}\left(h\frac{\partial \eta}{\partial y}\right) = 0. \tag{2.18}$$

2.3 Governing Equation for the Current Problem

The geometry for the propagation of a long wave over a linearly sloping beach is depicted in Figure 2.2 by defining x as the onshore direction –the direction from the shore towards the open sea–, with $x = 0$ defining the shoreline, and y as the longshore direction –direction parallel to the shore –. The domain of x is $[0, \infty)$ and the domain of y is $(-\infty, \infty)$.

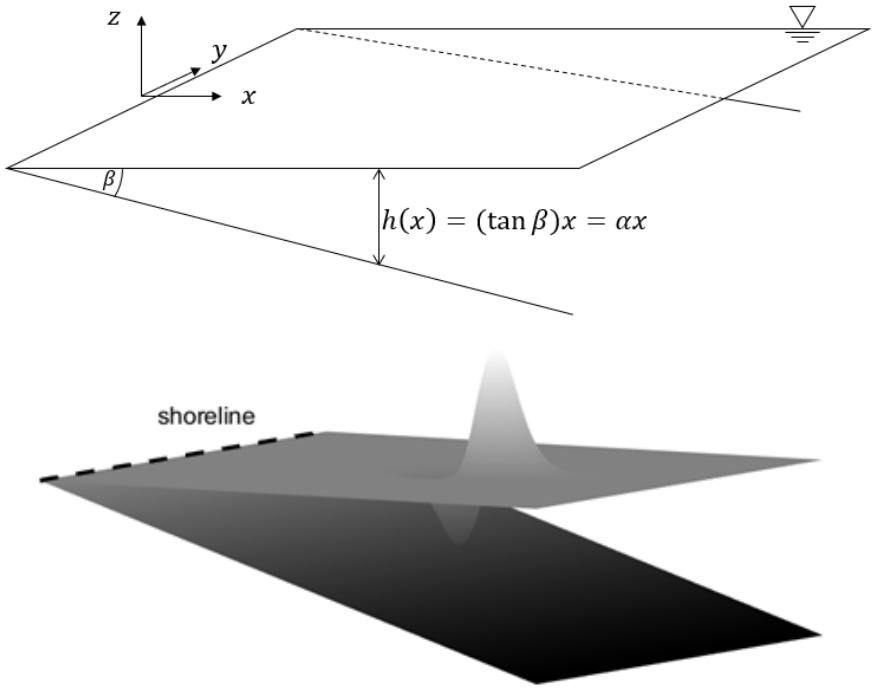

Figure 2.2: Definition sketch.

Now, Equation 2.18 becomes

$$\frac{\partial^2 \eta}{\partial t^2} - g\frac{\partial}{\partial x}\left(\alpha x \frac{\partial \eta}{\partial x}\right) - g\frac{\partial}{\partial y}\left(\alpha x \frac{\partial \eta}{\partial y}\right) = 0, \tag{2.19}$$

by considering linearly sloping beach, i.e., $h = \tan\beta\, x = \alpha x$, where β is the beach angle and α is the slope of the beach. The differential equation, Equation 2.19, is the governing equation for the problem considered. For convenience, the equation will be nondimensionalized. Using l_0 and αl_0 as horizontal and vertical characteristic length scales, respectively, and $\sqrt{l_0/g\alpha}$ as the characteristic time scale, i.e.,

$$(\tilde{x}, \tilde{y}) = \frac{(x, y)}{l_0}, \quad (\tilde{\eta}, \tilde{h}) = \frac{(\eta, h)}{\alpha l_0}, \quad \text{and} \quad \tilde{t} = \frac{t}{\sqrt{l_0/g\alpha}}. \tag{2.20}$$

Applying this scaling to Equation 2.19 results in

$$\frac{\partial^2 \tilde{\eta}}{\partial \tilde{t}^2} - \frac{\partial}{\partial \tilde{x}}\left(\tilde{x}\frac{\partial \tilde{\eta}}{\partial \tilde{x}}\right) - \frac{\partial}{\partial \tilde{y}}\left(\tilde{x}\frac{\partial \tilde{\eta}}{\partial \tilde{y}}\right) = 0, \tag{2.21}$$

the final non-dimensional form of the governing partial differential equation. Further on, the "$\sim$" sign will be dropped for convenience.

2.4 Solution of the Governing Equation

Equation 2.21 is a second-order linear partial differential equation with three independent variables. The Fourier transform will be applied in the y-direction (longshore direction) to reduce the number of variables. Since the domain of y is assumed to be $(-\infty, \infty)$, the initial wave may be considered symmetric with respect to the line $y = 0$. Thus, instead of the complex Fourier transform, the Fourier cosine transform will be employed. The Fourier cosine transform and inverse transform are defined as

$$\hat{\eta} = \int_0^\infty \eta \cos(ky) dy \quad \text{and} \quad \eta = \frac{2}{\pi}\int_0^\infty \hat{\eta}\cos(ky)dk, \tag{2.22}$$

respectively, where $\hat{\eta}$ is the transform of η, and k is the nondimensional wavenumber in the y-direction. Since the derivative and integral operators of the Fourier transform are linear, the transformation of Equation 2.21 is straightforward. The details are omitted for brevity. However, it is worth mentioning that the term $\partial\eta(x, 0, t)/\partial y$, which arises from the transform of $\partial^2\eta/\partial y^2$, is taken to be zero. The symmetry of the profile with respect to $y = 0$ justifies this. Then, the transformed equation is

$$\frac{\partial^2 \hat{\eta}}{\partial t^2} - \frac{\partial}{\partial x}\left(x\frac{\partial \hat{\eta}}{\partial x}\right) + xk^2\hat{\eta} = 0. \tag{2.23}$$

This governing equation will be considered with an initial profile, $\eta(x, y, 0)$, initially at rest, which leads to the following conditions,

$$\eta(x, y, 0) = \eta_i(x, y) \quad \text{and} \quad \left.\frac{\partial \eta(x, y, t)}{\partial t}\right|_{t=0} = 0. \tag{2.24}$$

Equation 2.23 is separable, since there are no cross-derivatives. Assuming $\hat{\eta}(x, t) = F(x)T(t)$ leads to

$$\frac{\partial^2 [F(x)T(t)]}{\partial t^2} - \frac{\partial}{\partial x}\left(x\frac{\partial [F(x)T(t)]}{\partial x}\right) + xk^2F(x)T(t) = 0, \tag{2.25}$$

and, in turn

$$F\frac{d^2T}{dt^2} - xT\frac{d^2F}{dx^2} - T\frac{dF}{dx} + xk^2FT = 0. \tag{2.26}$$

Separating the expressions after dividing by FT results in

$$\frac{1}{T}\frac{d^2T}{dt^2} = x\frac{1}{F}\frac{d^2F}{dx^2} + \frac{1}{F}\frac{dF}{dx} - xk^2 = c. \tag{2.27}$$

Equation 2.27 can only be valid if the expressions on the right- and left-hand-side are equal to the same constant, c. Due to the neglection of viscosity, the waves will not decay with respect to time. Therefore, it can be assumed that the solution with respect to time will be oscillatory, i.e., no decay. Hence, the constant is assumed to be $c = -\omega^2$, where ω is a real number. Therefore, Equation 2.27 turns into the following set of ordinary differential equations;

$$\frac{d^2T}{dt^2} + \omega^2 T = 0, \tag{2.28a}$$

$$x\frac{d^2F}{dx^2} + \frac{dF}{dx} - (xk^2 - \omega^2)F = 0. \tag{2.28b}$$

Equation 2.28a is a second-order linear ordinary differential equation with constant coefficients. Its solution is

$$T(t) = C_1\cos(\omega t) + C_2\sin(\omega t). \tag{2.29}$$

Equation 2.28b is a second-order linear differential equation with varying coefficients. It is expected that the wave decays as it propagates in the x-direction. Hence, the solution of $F(x)$ will be of the form $F(x) = e^{-a^2x}G(x)$, where a is some real number. The overall aim is to transform Equation 2.28b into a well-known differential equation. The transformation $F(x) = e^{-kx}G(2kx)$ is used (Fujima, Dozono, and Shigemura, 2000; Renzi and Sammarco, 2010). For convenience, the new variable $\varsigma = 2kx$ is introduced, i.e., $F(\varsigma/2k) = e^{-\varsigma/2}G(\varsigma)$. Hence, Equation 2.28b becomes

$$\varsigma\frac{d^2G}{d\varsigma^2} + (1-\varsigma)\frac{dG}{d\varsigma} - \left(\frac{1}{2} - \frac{\omega^2}{2k}\right)G = 0. \tag{2.30}$$

Equation 2.30 is known as the confluent hypergeometric equation, also known as Kummer's equation (Abramowitz and Stegun, 1970). Its solution is given in terms of the confluent hypergeometric functions of the first and second kind, $M(a,b,z)$ and $U(a,b,z)$, respectively. Hence,

$$G(\varsigma) = C_3M(\zeta,1,\varsigma) + C_4U(\zeta,1,\varsigma), \tag{2.31}$$

where $\zeta = (1 - \omega^2/k)/2$. However, the hypergeometric function of the second kind, U, is not bounded at $\varsigma = 0$ ($x = 0$). Therefore, it follows that the constant C_4 must be zero. Then, the solution reduces to

$$G(\varsigma) = C_3 M\left(\zeta, 1, \varsigma\right). \tag{2.32}$$

Thus, $F(x)$ is found to be

$$F(x) = C_3 e^{-kx} M(\zeta, 1, 2kx). \tag{2.33}$$

Recalling that $\hat{\eta}$ was defined as $F(x)T(t)$, the general solution becomes

$$\hat{\eta}(x, k, t) = \left[A\cos(\omega t) + B\sin(\omega t)\right] e^{-kx} M(\zeta, 1, 2kx), \tag{2.34}$$

where A and B represent the unknowns C_1C_3 and C_2C_3, respectively. The equation is simplified even further by making use of the initial condition, $\partial\eta/\partial t = \partial\hat{\eta}/\partial t = 0$, which leads to

$$\left.\frac{\partial\hat{\eta}}{\partial t}\right|_{t=0} = \omega B e^{-kx} M(\zeta, 1, 2kx) = 0. \tag{2.35}$$

B must equal zero for this equation to be satisfied, which reduces Equation 2.34 to

$$\hat{\eta} = A\cos\left(\omega t\right) e^{-kx} M(\zeta, 1, 2kx). \tag{2.36}$$

The differential equation (Equation 2.30) is a singular Sturm-Liouville problem with a regular singular point at $\varsigma = 0$. This means that there exists countably infinite eigenvalues, and corresponding eigenfunctions (Boyce, DiPrima, and Meade, 2021). Furthermore, the solution with respect to x must yield orthogonal eigenfunctions. Otherwise, the initial condition cannot be satisfied. Fujima, Dozono, and Shigemura (2000) states that the only way $\hat{\eta}$ is bounded if $\zeta = -n$, where n's are positive integers, as x tends to infinity. It is known that $M(-n, 1, x) = L_n(x)$, where $L_n(x)$ denote the Laguerre polynomial of order n (Abramowitz and Stegun, 1970). Equating ζ to $-n$ also leads to a dispersion relation. Hence, the n^{th} frequency and the n^{th} solution are

$$\omega_n = \sqrt{(2n+1)k}, \tag{2.37}$$

$$\hat{\eta}_n = A_n\cos\left(\omega_n t\right) e^{-kx} L_n(2kx), \tag{2.38}$$

respectively. Since the system is linear, the solution is nothing but the linear combination of all the possible solutions resulting in the general solution of

$$\hat{\eta} = \sum_{n=0}^{\infty} A_n\cos\left(\sqrt{(2n+1)k}t\right) e^{-kx} L_n(2kx). \tag{2.39}$$

The constants A_n must be determined to complete the solution. The initial condition in the form of $\eta(x, y, 0) = \eta_i(x, y) = \eta_o(x)\,\eta_\ell(y)$ will be used to find these coefficients. The choice of this form of initial condition will be discussed in Section 2.5. Since this condition is defined in the physical domain, it must first be transformed. The transformed variable is defined as $\hat{\eta}_i = \eta_o(x)\,\hat{\eta}_\ell(k)$, where $\hat{\eta}_\ell(k)$ is the Fourier-cosine transform of $\eta_\ell(y)$. Equation 2.39 leads to

$$\sum_{n=0}^{\infty} A_n e^{-kx} L_n(2kx) = \eta_o(x)\hat{\eta}_\ell(k), \tag{2.40}$$

at $t = 0$. Here, orthogonality of Laguerre polynomials with respect to the weight function e^{-x} will be employed expressing as,

$$\int_0^{\infty} e^{-x} L_n(x) L_m(x) dx = \delta_{nm}, \tag{2.41}$$

where δ_{nm} is the Kronecker delta (Abramowitz and Stegun, 1970). This is scaled to be consistent with the solution (Equation 2.39) to get

$$\int_0^{\infty} e^{-2kx} L_n(2kx) L_m(2kx) dx = \frac{\delta_{nm}}{2k}. \tag{2.42}$$

Multiplying both sides of Equation 2.40 with $e^{-kx} L_n(2kx)$, then integrating from 0 to ∞ gives

$$\frac{1}{2k} A_n = \hat{\eta}_\ell(k) \int_0^{\infty} \eta_o(x) e^{-kx} L_n(2kx) dx. \tag{2.43}$$

Thus, A_n's are obtained, and hence, $\hat{\eta}$ has been constructed. Then, the inverse Fourier-cosine transform is applied to find η. Hence, the final form of the solution is

$$\eta = \sum_{n=0}^{\infty} \frac{2}{\pi} \int_0^{\infty} A_n(k) e^{-kx} L_n(2kx) \cos\left(\sqrt{(2n+1)k}\, t\right) \cos(ky) dk, \tag{2.44}$$

where

$$A_n(k) = 2k\hat{\eta}_\ell(k) \int_0^{\infty} \eta_o(\xi) e^{-k\xi} L_n(2k\xi) d\xi. \tag{2.45}$$

Here the integration variable of the integral in $A_n(k)$ was changed from x to ξ to avoid confusion.

2.5 Initial Condition

One additional purpose of this study is to observe focusing mechanism as was observed by Kânoğlu et al. (2013) for the propagation of two-dimensional *N*-wave type

initial wave over a constant depth topography. Hence, a similar initial profile will be considered here. However, the solution is versatile and could be used for different types of initial profiles. *N*-wave type initial profile was first introduced by Tadepalli and Synolakis (1994) in one-dimension. Later, Kânoğlu et al. (2013) extended the *N*-wave definition to two-dimensional case. Following the definition by Kânoğlu et al. (2013), the initial profile thus reads

$$\begin{aligned}\eta_i = \eta_o(x) \times \eta_\ell(y) =& \frac{\varepsilon H}{2}(x - x_2)\,\mathrm{sech}^2\,\gamma(x - x_1) \\ & \times \left[\tanh\left(\gamma\left[y + L/2\right]\right) - \tanh\left(\gamma\left[y - L/2\right]\right)\right], \end{aligned} \tag{2.46}$$

where H and ε determine the wave height, x_1 and x_2 determine the location of the elevation and depression, γ is a constant that determines the frontal slope of the wave, and L is the wave crest length. One example of an initial profile is provided in Figure 2.3a.

The evaluation of the Fourier-cosine transform of Equation 2.46 with respect to y is given in Appendix A. The transformed initial condition is found to be

$$\hat{\eta}_i = \frac{\varepsilon H \pi}{2\gamma}(x - x_2)\,\mathrm{sech}^2[\gamma(x - x_1)]\sin\left(\frac{L}{2}k\right)\mathrm{csch}\left(\frac{\pi}{2\gamma}k\right). \tag{2.47}$$

Using the initial condition in Equation 2.45, the coefficients $A_n(k)$ are found as

$$\begin{aligned} A_n(k) =& 2k\frac{\varepsilon H \pi}{2\gamma}\sin\left(\frac{L}{2}k\right)\mathrm{csch}\left(\frac{\pi}{2\gamma}k\right) \\ & \times \int_0^\infty (\xi - x_2)\,\mathrm{sech}^2[\gamma(\xi - x_1)]e^{-k\xi}L_n(2k\xi)d\xi. \end{aligned} \tag{2.48}$$

Hence, the general solution, Equation 2.18, becomes

$$\begin{aligned}\eta(x,y,t) = \frac{2\varepsilon H}{\gamma}\sum_{n=0}^{\infty}\int_0^\infty & C_n(k)\,k\,\sin\left(\frac{L}{2}k\right)\mathrm{csch}\left(\frac{\pi}{2\gamma}k\right)\cos\left(\sqrt{(2n+1)}kt\right) \\ & \times \cos\left(ky\right)e^{-kx}L_n(2kx)dk, \end{aligned} \tag{2.49}$$

where

$$C_n(k) = \int_0^\infty (\xi - x_2)\,\mathrm{sech}^2\,\gamma(\xi - x_1)e^{-k\xi}L_n(2k\xi)d\xi. \tag{2.50}$$

Equation 2.49 is the final solution for the wave height. The solution is quite complicated, involving integrals over variables that cannot be separated into distinct functions of their own. While Laguerre polynomials can take large values for higher

orders, the sech function tends to zero, as $x \to \infty$. The integrand is also highly oscillatory. These properties of the integrand(s) make numerical integration difficult.

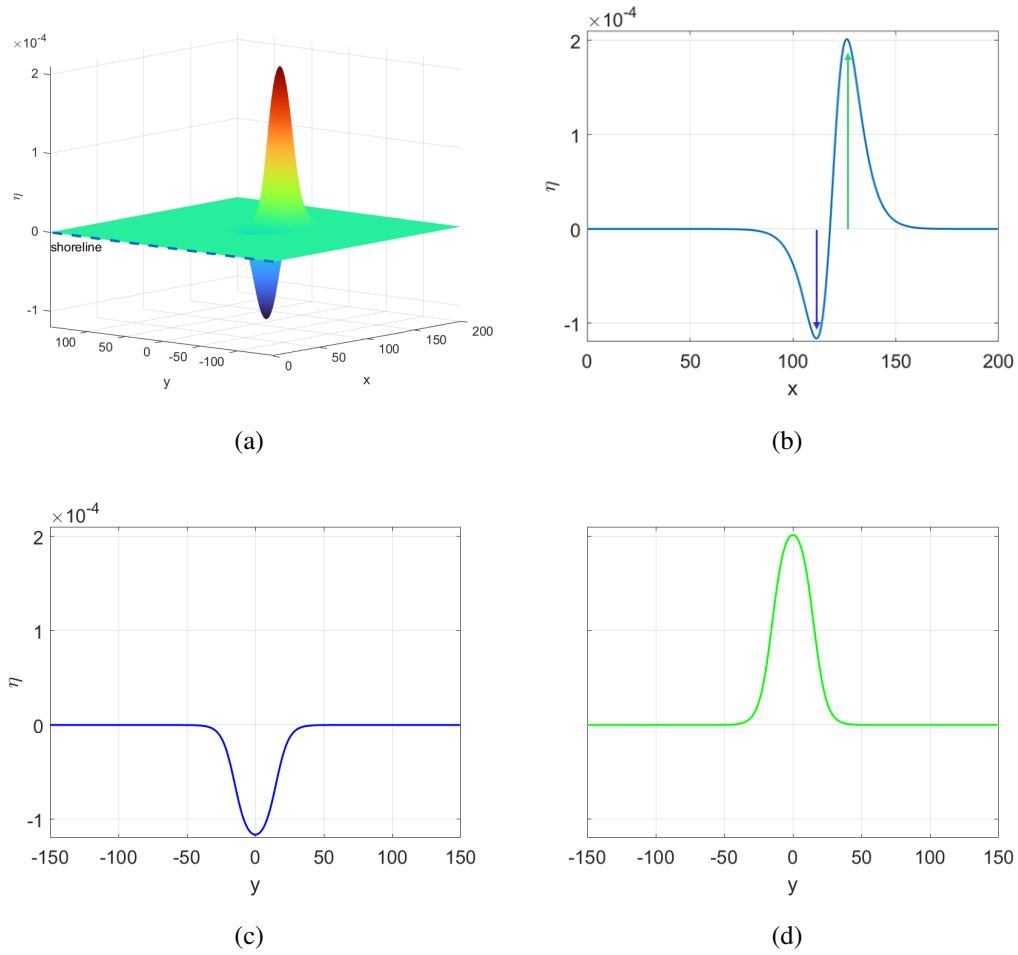

Figure 2.3: (a) Three-dimensional view of an initial profile having a finite crest length. The parameters are: $\varepsilon = 0.04$, $H = 0.001$, $\gamma = 0.106$, $x_1 = 120$, $x_2 = 118$, and $L/2 = 15$. The shoreline corresponds to the line $x = 0$, with this positioning of coordinates. Transect along (b) the bisector line (onshore direction). Transects along longshore direction at (c) the maximum, and (d) the minimum waveheight locations.

CHAPTER 3

RESULTS AND DISCUSSION

The solution integral, Equation 2.49, will be evaluated numerically in this chapter. The numerical evaluation of the two integrals involved in the solution is a challenging task due to the complexity of the integrands. Three methods, the Gauss-Legendre and the Gauss-Laguerre quadratures, and the computation of Laguerre expansions coefficients will be discussed in the following sections.

3.1 Solution with Gauss-Legendre Quadrature

The Legendre polynomials are orthogonal in the $[-1, 1]$ region with respect to the weight function $w = 1$. This relationship is expressed as

$$\int_{-1}^{1} P_m(x)P_n(x)dx = \begin{cases} \dfrac{2}{2n+1}, & \text{if } m = n, \\ 0, & \text{if } m \neq n. \end{cases} \tag{3.1}$$

The Gauss-Legendre quadrature of order n uses the roots of the Legendre polynomials of the same order as nodes. These nodes are given to be between

$$\cos\left(\frac{2i-1}{2n+1}\pi\right) \leq x_i \leq \cos\left(\frac{2i}{2n+1}\pi\right), \tag{3.2}$$

where n is the order of the polynomial and i denotes the i^{th} root (Abramowitz and Stegun, 1970). The quadrature weights are calculated using the following expression;

$$w_i = \frac{2}{(1-x_i^2)[P_n'(x_i)]^2}, \tag{3.3}$$

where $'$ denotes the derivative with respect to x (Abramowitz and Stegun, 1970). The integral of a function, $f(x)$, is thus approximated by the quadrature

$$\int_{-1}^{1} f(x)dx \approx \sum_{i=0}^{n} w_i f(x_i), \tag{3.4}$$

in the interval $[-1, 1]$. Extension of this integral to the integral over any finite interval, $[a, b]$, is achieved through the following linear transformation

$$x = \frac{b-a}{2}\xi + \frac{b+a}{2}. \tag{3.5}$$

Applying this transformation to the integral $\int_a^b f(x)dx$ gives

$$\int_a^b f(x)dx = \frac{b-a}{2}\int_{-1}^{1} f\left(\frac{b-a}{2}\xi + \frac{b+a}{2}\right)d\xi. \tag{3.6}$$

Thus, the approximation of the integral of a function over a finite region $[a, b]$ is

$$\int_a^b f(x)dx \approx \frac{b-a}{2}\sum_{i=0}^{n} w_i f\left(\frac{b-a}{2}\xi_i + \frac{b+a}{2}\right). \tag{3.7}$$

Here, ξ_i is the i^{th} root of the Legendre polynomial of order n.

Propagation of the initial profile given in Section 2.5 over a sloping beach is now calculated using Gauss-Legendre quadrature. Since the integrand decays rapidly, the integral is truncated to a finite interval. The transformation introduced in Equation 3.5 linearly transforms the weights and roots given by Equations 3.2 and 3.3. The comparison of the transects of the initial profile (Equation 2.47) and the solution at $t = 0$ is given in Figure 3.1. As can be seen, there is a clear difference between the definition and the computed value. The discrepancy is even more prominent in the longshore direction. The discrepancy is even more prominent in the longshore direction, maybe because of an increase in the value of y results in a more oscillatory integrand (due to the $\cos(ky)$ term).

The propagation is investigated even though there is a discrepancy in the reconstruction of the initial wave profile. The time evolution in $0 \leq t \leq 4.5$ is obtained at time intervals of $\Delta t = 0.50$ and presented in Figure 3.2. (Kânoğlu et al., 2013) points out that "...propagation produces waves propagating with different elevation and depression heights in each direction, along the bisector. Moreover, because of focusing,

the wave height increases at first on the leading-depression side, and then decreases monotonically. On the leading-elevation side, the decay is monotonous."

Here, leading depression N-wave and leading elevation N-wave propagates in opposite directions, as observed by (Kânoğlu et al., 2013) for the propagation over a constant depth. Further assertions can only be made through a more detailed study of the problem. However, it should be noted that the wave in the depression side, i.e., the wave moving towards the shore, does not decay as much as it does for the constant depth solution (Kânoğlu et al., 2013) due to shoaling.

Also, the wave height at the depression side initially decreases, then increases, before decreasing again. Though an increase in wave height may be caused by shoaling, this does not seem to be the case because the wave height would not decrease again afterward. This decrease may be attributed to the finite nature of the problem, i.e., the wave propagation in the longshore direction. It can be conjectured that focusing occurs due to the initial increase in wave height.

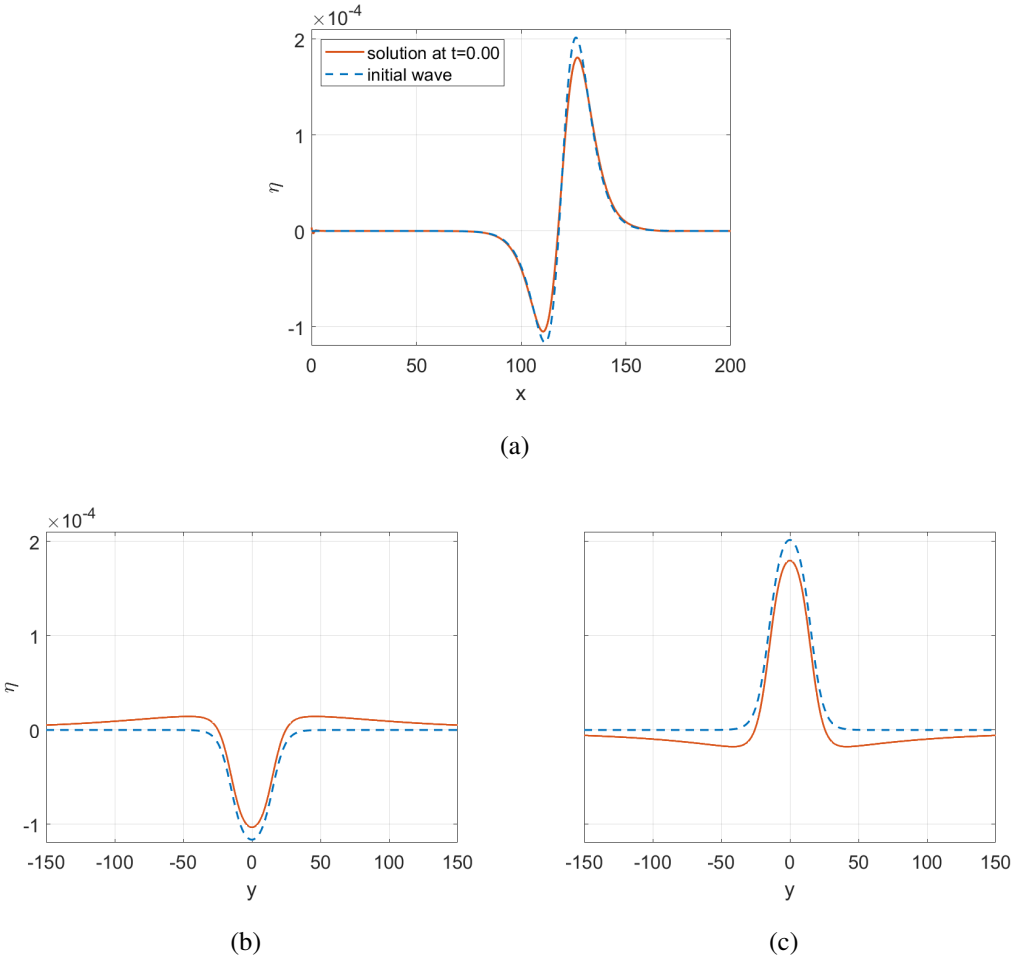

Figure 3.1: (a) The bisector transect along the onshore direction. The longshore transects along (b) the minimum and (c) the maximum wave height locations. The number of terms summed is $n = 180$. Two-hundred nodes were used for the outer integral, while hundred nodes were used for the inner integral. The parameters for the initial wave profile are: $\varepsilon = 0.04$, $H = 0.001$, $\gamma = 0.106$, $x_1 = 120$, $x_2 = 118$, and $L/2 = 15$.

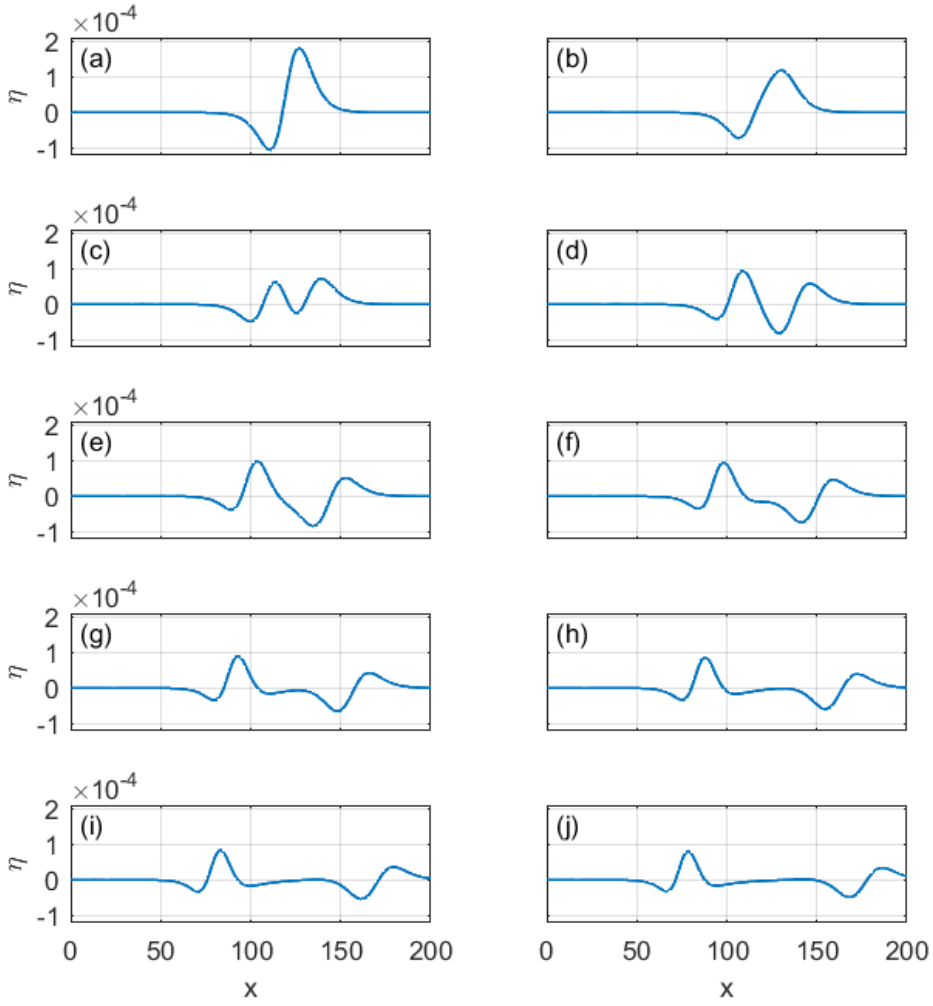

Figure 3.2: Transects along the bisector for times (a) $t = 0.00$, (b) $t = 0.50$, (c) $t = 1.00$, (d) $t = 1.50$, (e) $t = 2.00$, (f) $t = 2.50$, (g) $t = 3.00$, (h) $t = 3.50$, (i) $t = 4.00$, and (j) $t = 4.50$. The solution is obtained using the Gauss-Legendre quadrature. The number of nodes and initial wave parameters are given in the caption of Figure 3.1.

3.2 Solution with Gauss-Laguerre Quadrature

Another appropriate quadrature is the Gauss-Laguerre quadrature. This quadrature is especially useful in evaluating infinite integrals. Laguerre polynomials are orthonormal in the range $[0, \infty)$ for the weighting function e^{-x}, as mentioned, and this property is expressed as

$$\int_0^\infty e^{-x} L_m(x) L_n(x) dx = \delta_{mn}, \tag{3.8}$$

where δ_{mn} is the Kronecker delta (Abramowitz and Stegun, 1970). Hence, an integral of the form

$$\int_0^\infty e^{-x} f(x) dx, \tag{3.9}$$

can be approximated as

$$\int_0^\infty e^{-x} f(x) dx \approx \sum_{i=0}^{n} w_i f(x_i), \tag{3.10}$$

where x_i is the i^{th} root of the Laguerre polynomial of order n and w_i is the corresponding weight. According to Stroud and Secrest (1966), the values of the roots are closely approximated by

$$x_i = \begin{cases} \dfrac{3}{2.4n+1}, & \text{if } i = 0, \\ \dfrac{15}{2.5n+1} + x_0, & \text{if } i = 1, \\ \dfrac{[1+2.55(i+1)]}{1.9(i+1)}(x_{i-1} - x_{i-2}) + x_{i-1}, & \text{if } i > 1. \end{cases} \tag{3.11}$$

The weights are calculated using the following formula;

$$w_i = \frac{1}{x_i [L_n'(x_i)]^2}, \tag{3.12}$$

(Abramowitz and Stegun, 1970; Stroud and Secrest, 1966). Again, $'$ denotes derivative with respect to x. This quadrature is used to evaluate infinite integrals, as mentioned. However, Laguerre polynomials have poor resolution quality, as pointed out by Gottlieb and Orszag (1977). Laguerre polynomials' convergence rate is much slower as n increases compared to Legendre polynomials. Shen (2000) suggests that the argument, x, can be scaled so that the largest root of the Laguerre polynomial

corresponds to the value of the function, after which its values are negligible, to overcome this problem. Calling this value M and the largest root of the n^{th} order Laguerre polynomial x_n, the scaling factor is given as $\beta = M/x_n$. The original argument, x, will be replaced with $\beta x'$. This ensures that the largest node in Equation 3.10 of the integrand becomes M.

Integrands that cannot be expressed in the form $e^{-x}f(x)$ can still be integrated using this quadrature method. Given an integrand $g(x)$, this can be expressed as $e^{-x}e^{x}g(x)$. The new function $e^{x}g(x)$ can then be interpreted as $f(x)$. It should be noted that this function is computationally challenging. Because, as x increases, the product of a substantial function (e^{x}) and a minimal function ($g(x)$) must be computed, which will lead to significant errors. Therefore, it is often wise to try and merge the positive exponential with $g(x)$. Different types of integrals (all from 0 to ∞) are evaluated in Appendix B using the scaled and unscaled quadratures to demonstrate the reliability of this scaled quadrature method. The tests show that the scaled quadrature gives quite reliable results. Thus, Equation 2.49 can be evaluated using this method.

Calling the scaling factor for the inner integral of μ, and the scaling factor for the outer integral β, Equation 2.49 takes the form of

$$\eta(x,y,t) = \frac{2\varepsilon H}{\gamma}\sum_{n=0}^{\infty}\int_0^{\infty} C_n(\beta k)\beta k \sin\left(\frac{L}{2}\beta k\right)\operatorname{csch}\left(\frac{\pi}{2\gamma}\beta k\right) \times \cos\left(\sqrt{(2n+1)\beta k t}\right)\cos(\beta k y)e^{-\beta k x}L_n(2\beta k x)\beta dk, \tag{3.13}$$

where

$$C_n(\beta k) = \int_0^{\infty}(\mu\xi - x_2)\operatorname{sech}^2\left[\gamma(\mu\xi - x_1)\right]e^{-\beta k\mu\xi}L_n(2\beta k\mu\xi)\mu d\xi. \tag{3.14}$$

Multiplying the inner integrand with $e^{-\xi}e^{\xi}$ and the outer integrand with $e^{-k}e^{k}$ yields

$$\eta(x,y,t) = \frac{2\varepsilon H}{\gamma}\sum_{n=0}^{\infty}\int_0^{\infty} e^{-k}e^{k}C_n(\beta k)\beta k \sin\left(\frac{L}{2}\beta k\right)\operatorname{csch}\left(\frac{\pi}{2\gamma}\beta k\right) \times \cos\left(\sqrt{(2n+1)\beta k t}\right)\cos(\beta k y)e^{-\beta k x}L_n(2\beta k x)\beta dk, \tag{3.15}$$

with

$$C_n(\beta k) = \int_0^{\infty} e^{-\xi}e^{\xi}(\mu\xi - x_2)\operatorname{sech}^2\left[\gamma(\mu\xi - x_1)\right]e^{-\beta k\mu\xi}L_n(2\beta k\mu\xi)\mu d\xi. \tag{3.16}$$

The calculations are carried out as in the case of the Gauss-Legendre quadrature, and the results are given in Figures 3.3 and 3.4. As can be seen, the results are pretty similar to the ones obtained from the Gauss-Legendre quadrature. Even though more than a necessary number of terms are added, there is still some significant error. Similar conclusions can be drawn as in the Gauss-Legendre Quadrature solution, considering the results presented in Figure 3.4.

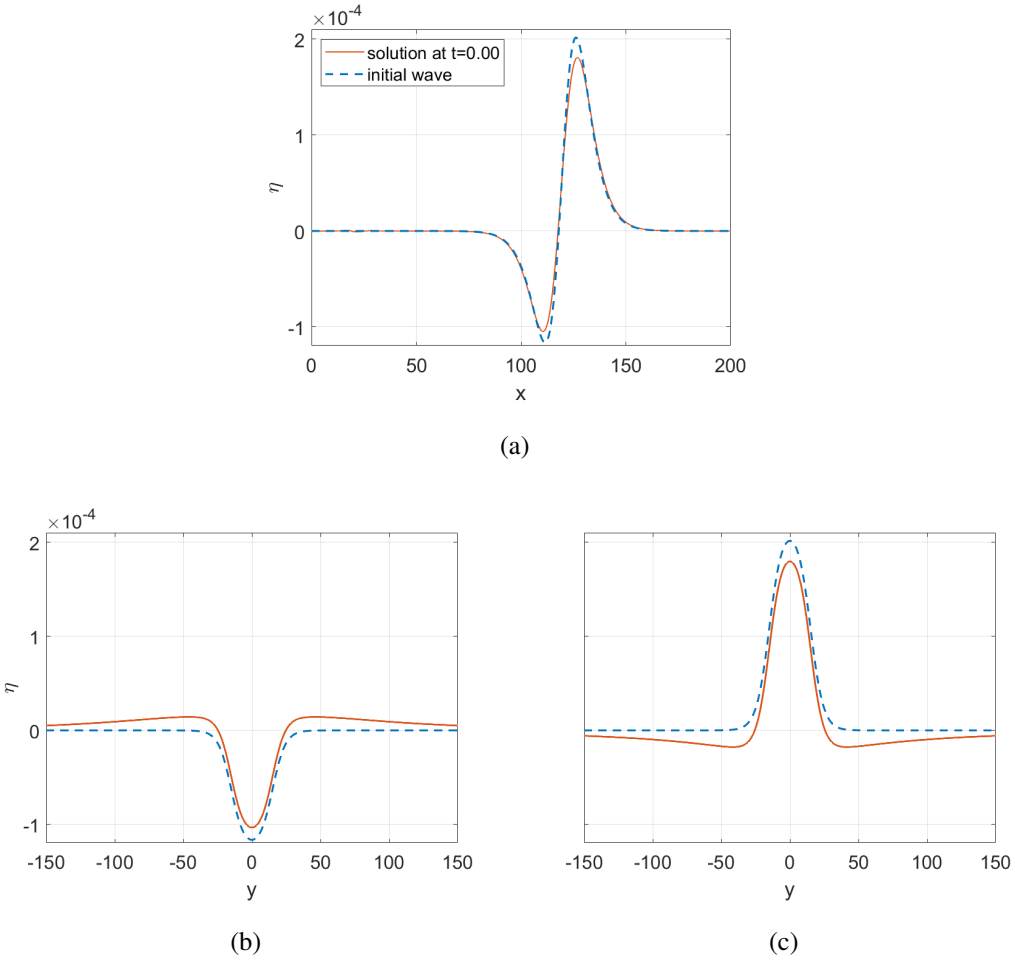

(a)

(b)

(c)

Figure 3.3: (a) The bisector transect along the onshore direction. The longshore transects along (b) the minimum and (c) the maximum wave height locations. The number of terms summed is $n = 180$. Ninety-four nodes were used for both the inner and outer integrals. The parameters for the initial wave profile are: $\varepsilon = 0.04$, $H = 0.001$, $\gamma = 0.106$, $x_1 = 120$, $x_2 = 118$, and $L/2 = 15$.

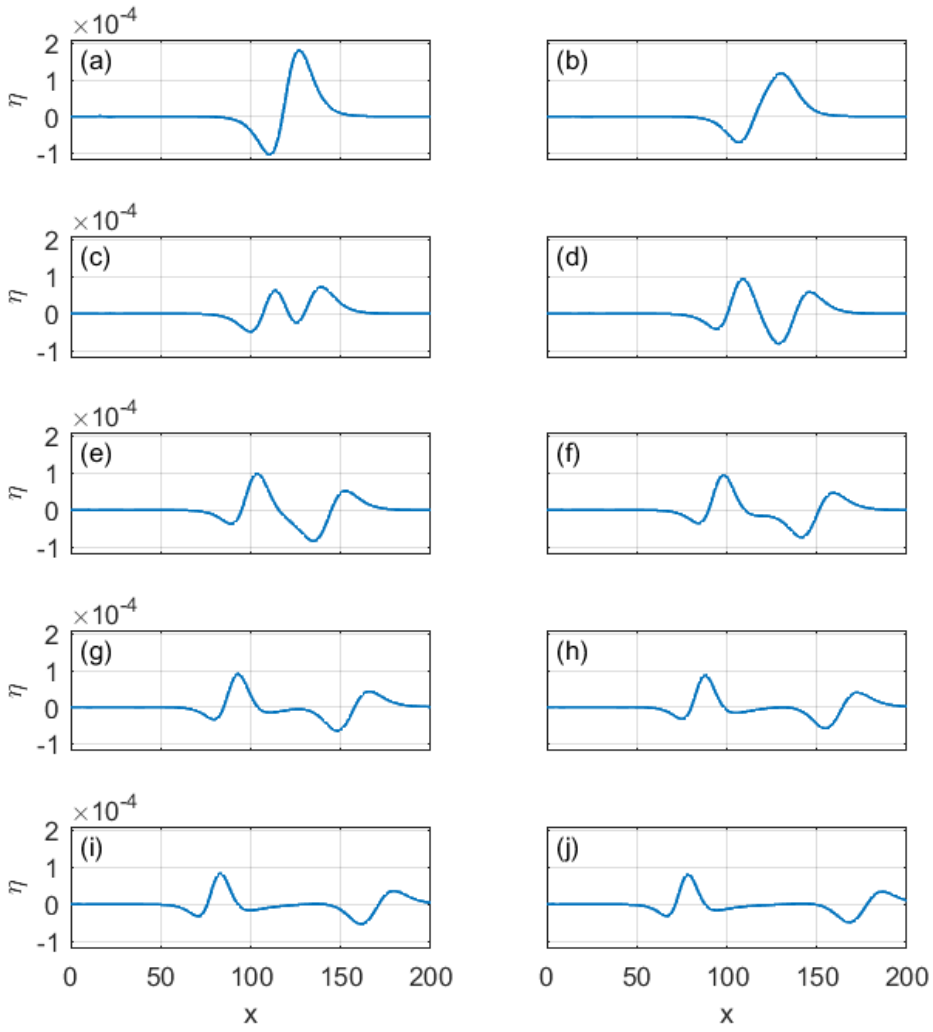

Figure 3.4: Transects along the bisector for times (a) $t = 0.00$, (b) $t = 0.50$, (c) $t = 1.00$, (d) $t = 1.50$, (e) $t = 2.00$, (f) $t = 2.50$, (g) $t = 3.00$, (h) $t = 3.50$, (i) $t = 4.00$, and (j) $t = 4.50$. The solution is obtained using the Gauss-Laguerre quadrature. The number of nodes and initial wave parameters are given in the caption of Figure 3.3.

3.3 Solution using Laguerre Expansion Coefficients

The integrands in Equations 2.49 and 2.50, except the $e^{-kx}L_n(2kx)$ terms, are expanded in terms of Laguerre polynomials, in this approach. Since Laguerre polynomials form an orthonormal basis in the range of $[0, \infty)$, any function $f(x)$ may be expressed as

$$f(x) = \sum_{n=0}^{\infty} a_n e^{-x/2} L_n(x). \tag{3.17}$$

The term $e^{-x/2}$ is included for computational reasons. The aim is to use readily available algorithms to evaluate the expansion coefficients, a_ns.

First, consider the inner integral;

$$C_n(k) = \int_0^{\infty} (\xi - x_2) \operatorname{sech}^2 \left[\gamma(\xi - x_1)\right] e^{-k\xi} L_n(2k\xi) d\xi. \tag{3.18}$$

Applying the transformation $z = 2k\xi$, this integral becomes

$$C_n(k) = \int_0^{\infty} \frac{1}{2k} \left(\frac{z}{2k} - x_2\right) \operatorname{sech}^2 \left[\gamma \left(\frac{z}{2k} - x_1\right)\right] e^{-z/2} L_n(z) dz. \tag{3.19}$$

Next, the function

$$f(z) = \frac{1}{2k} \left(\frac{z}{2k} - x_2\right) \operatorname{sech}^2 \left[\gamma \left(\frac{z}{2k} - x_1\right)\right], \tag{3.20}$$

i.e., the integrand except $e^{-z/2}L_n(z)$, is expanded in terms of Laguerre polynomials;

$$f(z) = \sum_{m=0}^{\infty} a_m e^{-z/2} L_m(z), \tag{3.21}$$

where $a_m = a_m(k)$. Then, Equation 3.19 leads to

$$C_n(k) = \int_0^{\infty} \sum_{m=0}^{\infty} a_m e^{-z/2} L_m(z) e^{-z/2} L_n(z) dz. \tag{3.22}$$

As can be seen immediately, due to the orthogonality of Laguerre polynomials, $C_n(k)$ reduces to

$$C_n(k) = a_n(k). \tag{3.23}$$

This is a neat way to express C_n, since

$$a_n = \int_0^{\infty} f(z) e^{-z/2} L_n(z) dz. \tag{3.24}$$

As for the outer integral,

$$\eta = \frac{2\varepsilon H}{\gamma}\sum_{n=0}^{\infty}\int_0^{\infty} C_n(k)\, k \sin\left(\frac{L}{2}k\right)\operatorname{csch}\left(\frac{\pi}{2\gamma}k\right)\cos\left(\sqrt{(2n+1)kt}\right)\cos\left(ky\right) \times e^{-kx}L_n(2kx)dk, \tag{3.25}$$

the transformation $\Omega = 2xk$ is applied, resulting in

$$\eta(x,y,t) = \frac{2\varepsilon H}{\gamma}\sum_{n=0}^{\infty}\int_0^{\infty}\frac{1}{2x}a_n\left(\frac{\Omega}{2x}\right)\frac{\Omega}{2x}\sin\left(\frac{L}{2}\frac{\Omega}{2x}\right)\operatorname{csch}\left(\frac{\pi}{2\gamma}\frac{\Omega}{2x}\right) \times \cos\left(\sqrt{(2n+1)\frac{\Omega}{2x}t}\right)\cos(\frac{\Omega}{2x}y)e^{-\frac{\Omega}{2}}L_n(\Omega)d\Omega. \tag{3.26}$$

Similarly, the function

$$g_n(\Omega) = \frac{a_n(\frac{\Omega}{2x})}{2x}\frac{\Omega}{2x}\sin\left(\frac{L\Omega}{4x}\right)\operatorname{csch}\left(\frac{\pi\Omega}{4\gamma x}\right)\cos\left(\sqrt{(2n+1)\frac{\Omega}{2x}t}\right)\cos\left(\frac{\Omega}{2x}y\right), \tag{3.27}$$

is expanded in terms of Laguerre polynomials, as in the case of $f(z)$. Note that $g_n(\Omega)$ has the subscript n. This is because it contains the coefficients a_n. These coefficients are dependent on the order of the Laguerre polynomial, hence, dependent on the index n. The expansion of g_n is

$$g_n(\Omega) = \sum_{m=0}^{\infty} b_{nm}e^{-\Omega/2}L_m(\Omega), \tag{3.28}$$

where $b_{nm} = b_{nm}(x,y,t)$. Using this expansion in Equation 3.26, one obtains

$$\eta(x,y,t) = \frac{2\varepsilon H}{\gamma}\sum_{n=0}^{\infty}\int_0^{\infty}\sum_{m=0}^{\infty} b_{nm}(x,y,t)e^{-\Omega/2}L_m(\Omega)e^{-\Omega/2}L_n(\Omega)d\Omega. \tag{3.29}$$

Due to the orthogonality of Laguerre polynomials, this equation simplifies to

$$\eta(x,y,t) = \frac{2\varepsilon H}{\gamma}\sum_{n=0}^{\infty} b_{nn}(x,y,t). \tag{3.30}$$

The term b_{nn} represents the coefficients of Laguerre expansions of the integrands. The double subscript arises due to the inner and outer integrals being both involve the summation indices.

The coefficients, a_n's and b_{nn}'s are calculated using "LaguerreEig", a Matlab m-file provided in Damian Trif (2022). The initial wave profile is calculated numerically and

compared with the actual profile. The reconstruction of the initial solution is more accurate than the results from the previous two methodologies. Its accuracy is easier to notice when the transects are compared (Figure 3.5). Minor discrepancies are visible in the 3D figure for larger y-values; however, they are insignificant. The number of terms taken in Equations 3.21 and 3.28 are 30, much less than the terms taken in the Gauss-Legendre and Gauss-Laguerre quadratures. Indeed, 30 terms should be more than enough to accurately calculate the wave profiles due to the exponentially decaying property of the Laguerre coefficients. However, when the Gauss-Legendre and Gauss-Laguerre quadratures are used, taking only 30 terms produced erroneous profiles.

The time evolution with different time steps is given in Figure 3.7. Again, focusing seems to be present. However, this method yields significantly different solutions from the previous ones. The most noticeable difference is that the amplitude values obtained via this method are significantly smaller than the amplitudes in the quadrature solutions, as the wave propagates along the x-direction. Furthermore, the overall shape of the waves for later times seems counter-intuitive, i.e., the irregular shapes seem to be physically wrong. Nevertheless, the 3D profiles are also plotted to help provide insight into these transects. The plots are given below.

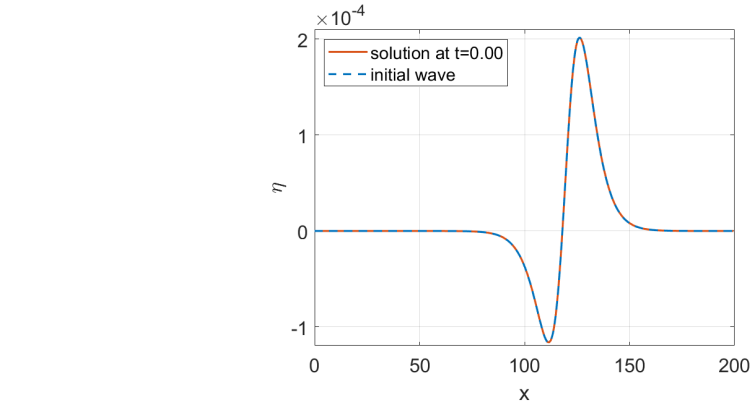

(a)

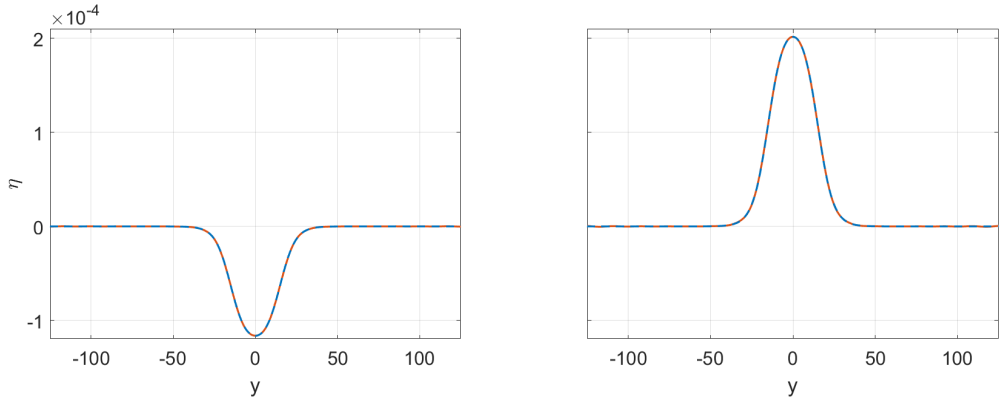

(b) (c)

Figure 3.5: (a) The bisector transect along the onshore direction. The longshore transects along (b) the minimum and (c) the maximum wave height locations. The number of terms summed is $n = 30$. The parameters for the initial wave profile are: $\varepsilon = 0.04$, $H = 0.001$, $\gamma = 0.106$, $x_1 = 120$, $x_2 = 118$, and $L/2 = 15$.

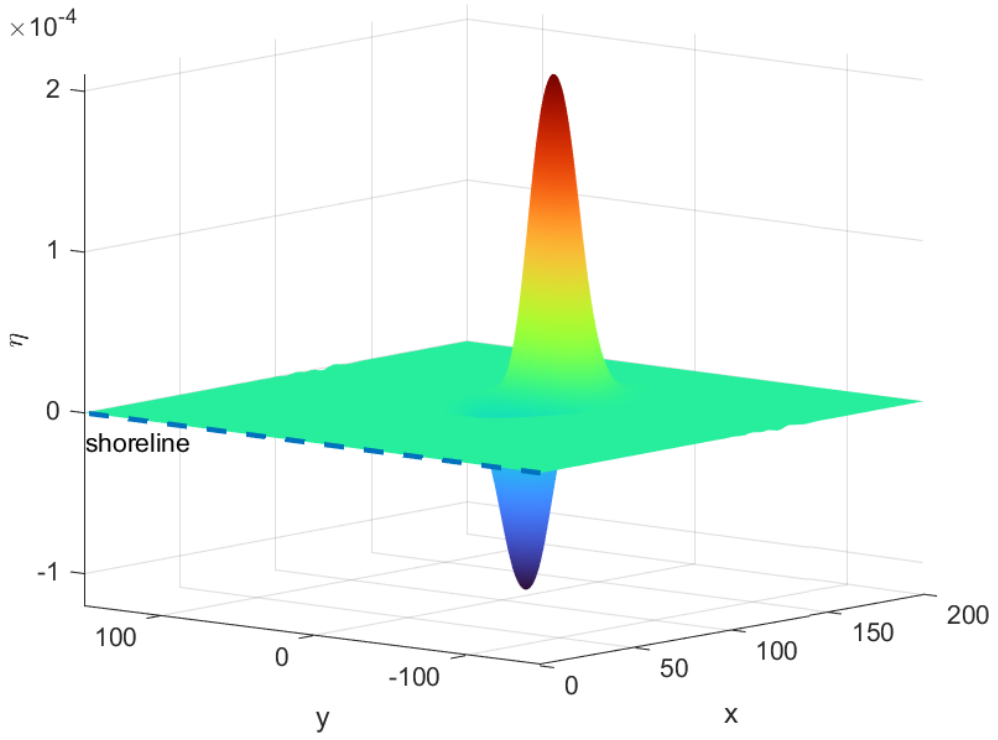

Figure 3.6: Solution for $t = 0.00$. Refer to Figure 3.5 for the values of the parameters.

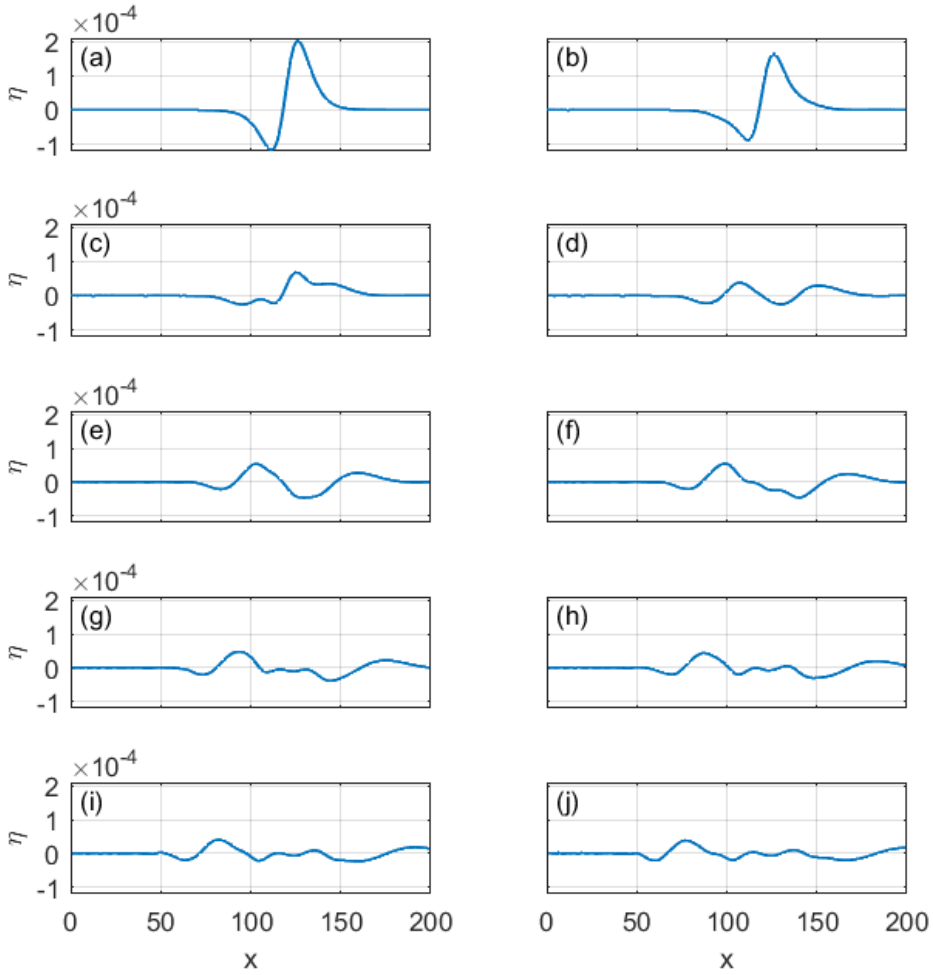

Figure 3.7: Transects along the bisector for times (a) $t = 0.00$, (b) $t = 0.50$, (c) $t = 1.00$, (d) $t = 1.50$, (e) $t = 2.00$, (f) $t = 2.50$, (g) $t = 3.00$, (h) $t = 3.50$, (i) $t = 4.00$, and (j) $t = 4.50$. The solutions are obtained using the Laguerre coefficient expansion method. The number of nodes and initial wave parameters are given in the caption of Figure 3.5.

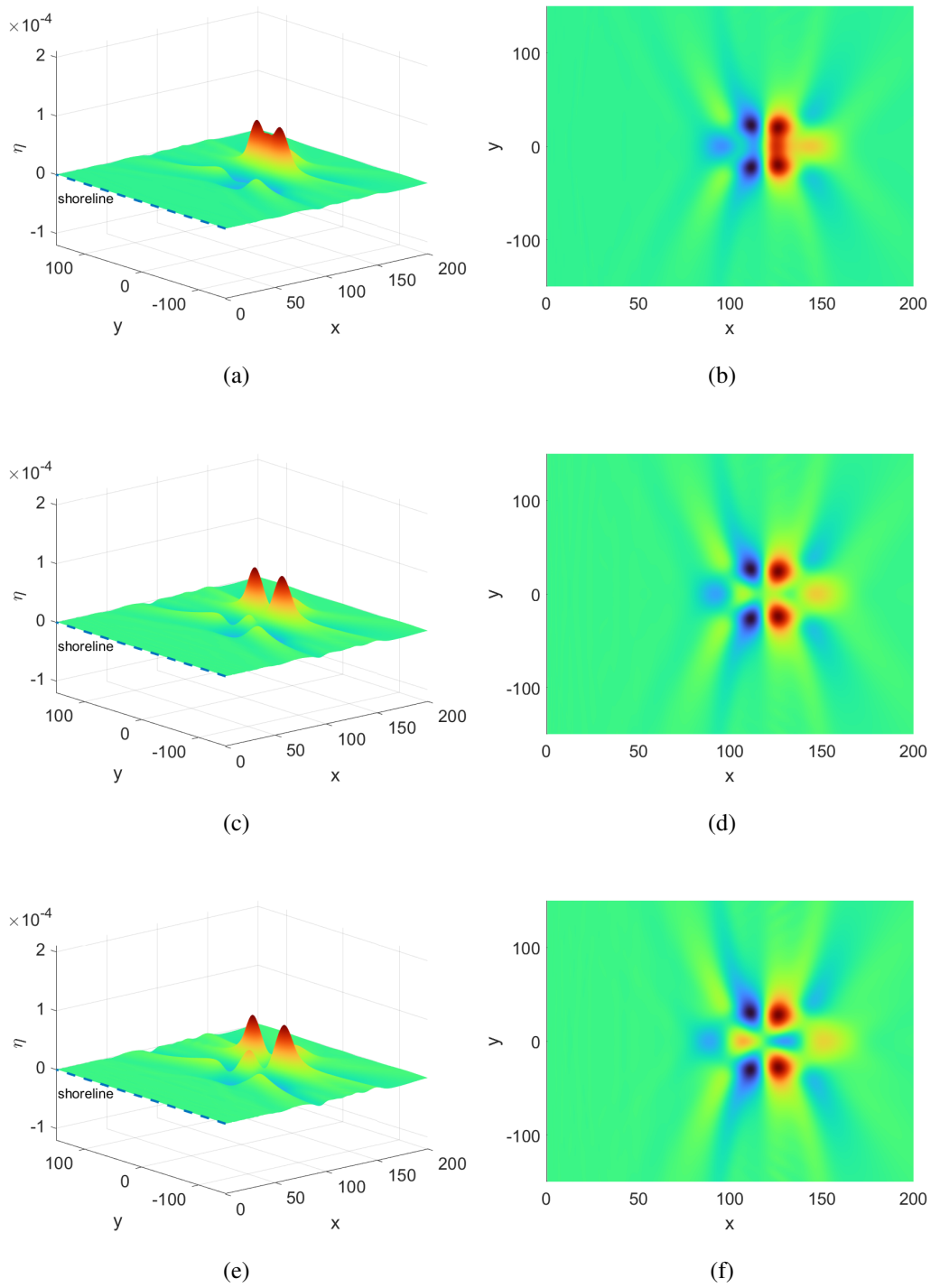

Figure 3.8: The three dimensional views and contour plots for times: (a) and (b) $t = 1.00$, (c) and (d) $t = 1.25$, and (e) and (f) $t = 1.50$. Refer to the caption of Figure 3.5 for the parameters.

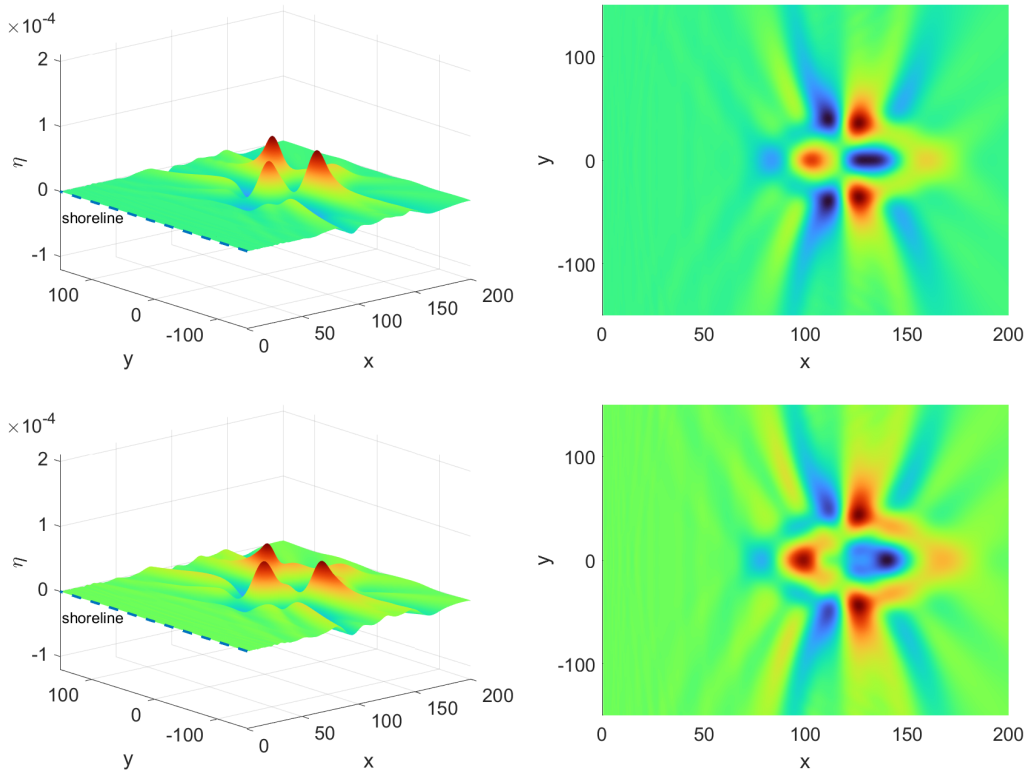

Figure 3.9: The three dimensional views and contour plots for times: (a) and (b) $t = 2.00$, and (c) and (d) $t = 2.50$. Refer to the caption of Figure 3.5 for the parameters.

CHAPTER 4

CONCLUSION

The linear shallow water-wave equations for two-spatial and one-temporal dimensions are reduced into a single PDE for the wave height, η, and solved analytically. The solution obtained is in the form two infinite integrals which can not be evaluated analytically. Therefore, the resultant solution for η is evaluated numerically, using the Gauss-Legendre quadrature, the Gauss-Laguerre quadrature, and Laguerre polynomial expansion. Among these, the Laguerre expansion method provides the best initial results, i.e., the initial profiles match perfectly, whereas the other two methods yield initial results with significant errors. However, the propagation patterns obtained by the Laguerre expansion method are quite counter-intuitive, while the quadrature solutions seem to produce more physically reasonable propagation characteristics. However, in all solutions there seems to be focusing taking place and the 3D views of the propagation support this, even though it has not been demonstrated with certainty. The difficulty in determining wave propagation behavior arises from the sensitivity of the solution to the parameters and numerical approaches. The solution algorithms must be improved. Furthermore, the solution must be validated from real-life events, experiments, and numerical solutions. All of these are topics for future work.

REFERENCES

References

Abramowitz, Milton and Irene A Stegun (1970). *Handbook of mathematical functions with formulas, graphs, and mathematical tables*.

Boyce, William E, Richard C DiPrima, and Douglas B Meade (2021). *Elementary differential equations and boundary value problems*. John Wiley & Sons.

Buhler, O. and K. Helfrich (2010). *2009 Program of Studies: Nonlinear Waves*. Tech. rep. 2010-01. Woods Hole, Massachusetts 02543: Woods Hole Oceanographic Institution. Chap. Lecture 8. URL: https://websites.pmc.ucsc.edu/~echen/Site/Publications_files/GFD_proc_2009.pdf.

Carrier, George F, Tai Tei Wu, and Harry Yeh (2003). "Tsunami run-up and drawdown on a plane beach". In: *Journal of Fluid Mechanics* 475, pp. 79–99.

Damian Trif (2022). *LaguerreEig, Retrieved 1 December*. MATLAB Central File Exchange. URL: https://www.mathworks.com/matlabcentral/fileexchange/24266-laguerreeig.

Fujima, Koji, Ryoichi Dozono, and Toshiyuki Shigemura (2000). "Generation and propagation of tsunami accompanying edge waves on a uniform sloping shelf". In: *Coastal Engineering Journal* 42(2), pp. 211–236.

Gottlieb, David and Steven A Orszag (1977). *Numerical analysis of spectral methods: theory and applications*. SIAM.

Gupta, Harsh K and Vineet K Gahalaut (2013). *Three Great Tsunamis: Lisbon (1755), Sumatra-Andaman (2004) and Japan (2011)*. Springer.

Kânoğlu, Utku et al. (2013). "Focusing of long waves with finite crest over constant depth". In: *Proceedings of the Royal Society A: Mathematical, Physical and Engineering Sciences* 469(2153), p. 20130015.

Levin, Boris W, Mikhail Nosov, et al. (2009). *Physics of tsunamis*. Vol. 2016. Springer.

Oberhettinger, Fritz (2012). *Tables of Fourier transforms and Fourier transforms of distributions*. Springer Science & Business Media.

Renzi, E and P Sammarco (2010). "Landslide tsunamis propagating around a conical island". In: *Journal of Fluid Mechanics* 650, pp. 251–285.

Sammarco, P and E Renzi (2008). "Landslide tsunamis propagating along a plane beach". In: *Journal of Fluid Mechanics* 598, pp. 107–119.

Shen, Jie (2000). "Stable and efficient spectral methods in unbounded domains using Laguerre functions". In: *SIAM Journal on Numerical Analysis* 38(4), pp. 1113–1133.

Stroud, Arthur H and Don Secrest (1966). *Gaussian Quadrature Formulas: By AH Stroud and Don Secrest*. Prentice-Hall.

Tadepalli, Srinivas and Costas Emmanuel Synolakis (1994). "The run-up of N-waves on sloping beaches". In: *Proceedings of the Royal Society of London. Series A: Mathematical and Physical Sciences* 445(1923), pp. 99–112.

Appendix A

FOURIER TRANSFORM OF THE HYPERBOLIC TANGENT

The Fourier sine transform of $\tanh(x)$ is given as

$$\int_0^\infty \tanh(x)\sin(kx)dx = \frac{\pi}{2}\,\mathrm{csch}\left(\frac{\pi}{2}k\right), \tag{A.1}$$

in Kânoğlu et al. (2013). This is equal to half the complex Fourier transform, i.e.,

$$\int_{-\infty}^\infty \tanh(x)e^{-ikx}dx = -i\pi\,\mathrm{csch}\left(\frac{\pi}{2}k\right). \tag{A.2}$$

Note that the negative imaginary unit, $-i$, was added because the Fourier-sine transform corresponds to the imaginary part of the complex Fourier transform. The function to be transformed is

$$\eta_\ell(y) = \tanh(\gamma[y + L/2]) - \tanh(\gamma[y - L/2]), \tag{A.3}$$

in Equation 2.46. This expression is an even function. Thus, the complex transform must equal twice of the cosine transform. Since the Fourier transform is a linear operation, the transform of both terms of η_ℓ will be evaluated separately and then the results will be subtracted. Therefore,

$$\begin{aligned}\int_{-\infty}^\infty \tanh(\gamma[y + L/2])e^{-iky}dy &= \int_{-\infty}^\infty \tanh(\gamma y')e^{-ik[y'-L/2]}dy' \\ = e^{iL/2}\int_{-\infty}^\infty \tanh(y')e^{-iky''/\gamma}\frac{dy''}{\gamma} &= -i\frac{\pi}{\gamma}e^{iL/2}\,\mathrm{csch}\left(\frac{\pi}{2\gamma}k\right),\end{aligned} \tag{A.4}$$

and carrying out a similar process for $\tanh(\gamma[y - L/2])$,

$$\int_{-\infty}^\infty \tanh(\gamma[y - L/2])e^{-iky}dy = -i\frac{\pi}{\gamma}e^{-iL/2}\,\mathrm{csch}\left(\frac{\pi}{2\gamma}k\right). \tag{A.5}$$

Subtracting the last two equations leads to the following

$$\int_0^\infty [\tanh(\gamma[y+L/2]) - \tanh(\gamma[y-L/2])]\cos(ky)dy = \frac{\pi}{\gamma}\sin\left(\frac{L}{2}k\right)\mathrm{csch}\left(\frac{\pi}{2\gamma}k\right). \tag{A.6}$$

for the cosine transform of η_ℓ.

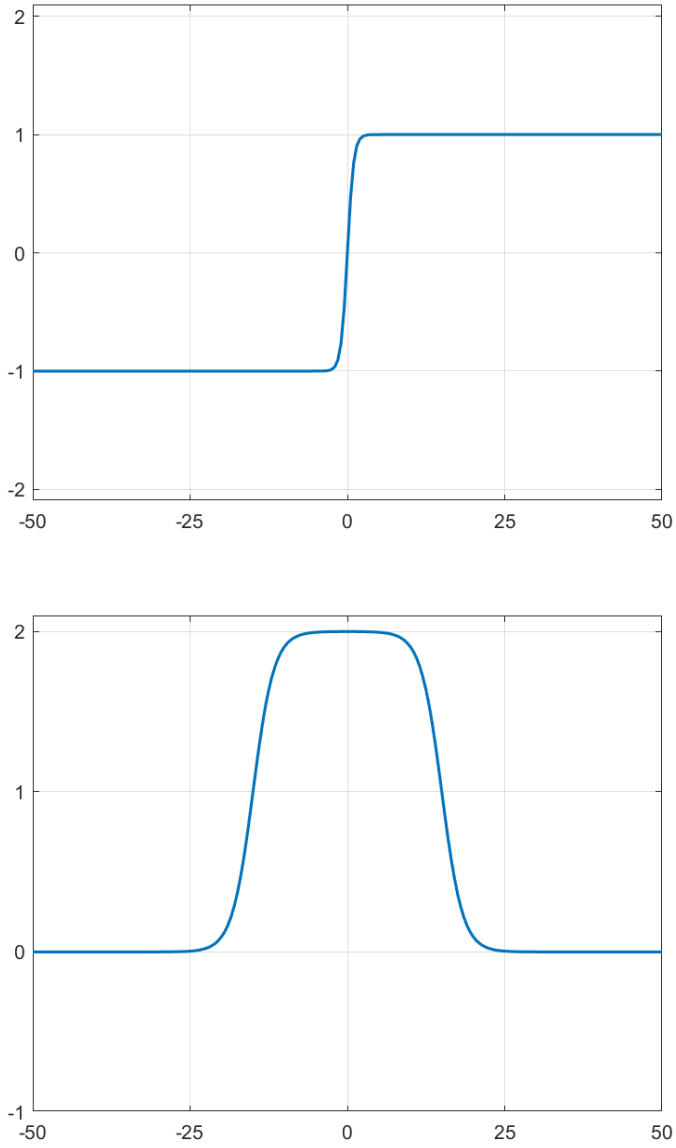

Figure A.1: Functions of: *(Top)* $\tanh(x)$ and *(Bottom)* $\tanh(0.5[x+15]) - \tanh(0.5[x-15])$.

Appendix B

EVALUATION OF INTEGRALS USING THE GAUSS-LAGUERRE QUADRATURE

B.1 Integrands Involving the Exponential Function

One of the most straightforward integrals that comes to mind is

$$\int_0^\infty e^{-x} dx. \tag{B.1}$$

Notice that this integral is the same as $\int_0^\infty e^{-x} L_0(x) L_0(x) dx$, since $L_0(x) = 1$. Hence, the solution is expected to be obtained accurately even if the order is $n = 1$. From Table B.1 it is clear that this is the case. This integral cannot be scaled because $f(x) = 1$ is significant in the whole domain.

Another integral that immediately comes to mind is the well known Gaussian integral,

$$\int_0^\infty e^{-x^2} dx = \frac{\sqrt{\pi}}{2}. \tag{B.2}$$

The integrand is manipulated and rewritten as

$$e^{-x} e^{-x(x-1)}. \tag{B.3}$$

This integral is also relatively simple. However, it converges slower than the previous one due to the previously mentioned spreading of the nodes/roots. For large x, the Gaussian e^{-x^2} tends towards zero very quickly, making additions of large x-values unnecessary. For $x = 5.0$, the value of e^{-x^2} is around 10^{-11}. Hence, using the scaling factor $\beta = 5/x_n$, the integral becomes $\int_0^\infty \beta e^{-\beta^2 x^2} dx$. The result obtained is given in Table B.2b. Note that even at $n = 10$, the error is small, whereas, for the unscaled

quadrature, similar errors are only reached when $n \approx 40$. However, note that as the order, n, increases, the unscaled quadrature yields more accurate results than the scaled solution, even though both results are quite accurate. This happens because the scaling factor becomes quite small with increasing order (since $5/x_n$ becomes smaller as x_n increases). Thus, if the integrand needed to be scaled between $[0, 1]$, for example, scaling would not always give better results. Therefore, one needs to take precautions when using scaling factors.

Order, n	Solution	Error, $\left\|\frac{(a-b)}{a}\right\|$
1	1.0000	0
2	1.0000	3.40e-13
3	1.0000	7.68e-12
4	1.0000	1.66e-11
5	1.0000	3.74e-11
6	1.0000	4.92e-11
7	1.0000	5.89e-11
8	1.0000	9.08e-13
9	1.0000	1.02e-11
10	1.0000	3.69e-12

Table B.1: Computations of $I = \int_0^\infty e^{-x} dx$ for different orders of Laguerre polynomials.

Order, n	Solution	Error, $\frac{(a-b)}{a}$
5	0.85578	0.0344
10	0.88656	0.000371
15	0.88635	0.00014
20	0.88620	2.83e-05
25	0.88623	4.2e-06
30	0.88623	3.62e-07
35	0.88623	7.74e-08
40	0.88623	5.63e-08
45	0.88623	1.90e-08
50	0.88623	3.86e-09
55	0.88623	1.23e-10
60	0.88623	2.56e-10
65	0.88623	9.58e-11
70	0.88623	1.19e-11
75	0.88623	7.38e-12
80	0.88623	1.49e-12
85	0.88623	9.47e-13
90	0.88623	7.94e-13
95	0.88623	2.81e-13
100	0.88623	1.92e-13

(a) Normal quadrature

Order, n	Solution	Error, $\frac{(a-b)}{a}$
5	0.88529	0.00106
10	0.88623	1.07e-08
15	0.88623	2.78e-11
20	0.88623	1.08e-10
25	0.88623	1.79e-10
30	0.88623	8.13e-11
35	0.88623	1.39e-10
40	0.88623	2.61e-10
45	0.88623	1.99e-10
50	0.88623	2.38e-10
55	0.88623	3.33e-10
60	0.88623	2.40e-10
65	0.88623	2.37e-10
70	0.88623	4.53e-10
75	0.88623	4.11e-10
80	0.88623	4.88e-10
85	0.88623	5.78e-10
90	0.88623	5.02e-10
95	0.88623	4.93e-10
100	0.88623	6.77e-10

(b) Scaled quadrature

Table B.2: Computations of $I = \int_0^\infty e^{-x^2} dx$ for different orders.

B.2 Integrands Involving Hyperbolic Functions

Integrals of hyperbolic functions are also of interest since they appear in Equation 2.49. Therefore, integrals of different forms of the $\mathrm{sech}(x)$ & $\mathrm{csch}(x)$ functions will be evaluated.

Given

$$\int \mathrm{sech}(x)dx = 2\arctan\left(\tanh\left[\frac{x}{2}\right]\right) + c, \tag{B.4}$$

it follows that $\int_0^\infty \mathrm{sech}(x)dx$ is $\pi/2$. Manipulating the integrand,

$$\mathrm{sech}(x)dx = \frac{2}{(e^x + e^{-x})} = \frac{2}{e^x(1 + e^{-2x})} = \frac{2e^{-x}}{(1 + e^{-2x})}. \tag{B.5}$$

Hence,

$$\int_0^\infty \mathrm{sech}(x)dx = \int_0^\infty e^{-x}\frac{2}{(1 + e^{-2x})}dx, \tag{B.6}$$

This integral is computed with and without a scaling factor. As can be seen in Table B.3, the solution with the scaling factor produces more accurate results for smaller quadrature orders. As the order increases, the results obtained from the scaled quadrature become less accurate than the unscaled quadrature, even though the result remains very accurate.

Next, the integral

$$\int \mathrm{sech}^2(x)dx = \tanh(x) + c, \tag{B.7}$$

is considered. This function does not have any significant value after $x = 15$, hence scaling is done accordingly. As can be seen from Table B.4, the scaled solution gives very accurate results much faster, again. The solution for $n = 15$ for the scaled quadrature is roughly equal to the solution for $n = 50$ for the unscaled one.

The integral $\int_0^\infty \mathrm{csch}(x)dx$ diverges, due to the singularity at $x = 0$. Therefore, this integral cannot be considered. Instead, the integral

$$\int_0^\infty x\,\mathrm{csch}(x)dx = \frac{\pi^2}{4}, \tag{B.8}$$

will be computed. The manipulations necessary to express the integrand as $e^{-x}f(x)$ will not be shown now or after this point, as it is trivial. In the scaled quadrature, the largest root will correspond to $x = 30$. The results are given in Table B.5. As can be seen, the standard and scaled quadratures both compute the result quite accurately. There is no significant difference in the convergence rate, i.e., the necessary orders are roughly the same.

Order, n	Solution	Error, $\left\lvert\frac{(a-b)}{a}\right\rvert$
5	1.5680	0.00179
10	1.5709	7.37e-05
15	1.5708	7.16e-06
20	1.5708	3.28e-07
25	1.5708	1.1e-07
30	1.5708	1.78e-08
35	1.5708	4.14e-09
40	1.5708	7.2e-10
45	1.5708	2.98e-10
50	1.5708	2.86e-11
55	1.5708	3.82e-11
60	1.5708	1.45e-11
65	1.5708	5.47e-12
70	1.5708	3.69e-12
75	1.5708	2.91e-12
80	1.5708	2.01e-12
85	1.5708	1.22e-12
90	1.5708	6.84e-13
95	1.5708	3.61e-13
100	1.5708	1.75e-13

(a) Normal quadrature

Order, n	Solution	Error, $\left\lvert\frac{(a-b)}{a}\right\rvert$
5	1.5826	0.00753
10	1.5708	2.29e-06
15	1.5708	2.19e-08
20	1.5708	1.01e-10
25	1.5708	5.09e-11
30	1.5708	3.39e-11
35	1.5708	1.12e-10
40	1.5708	1.01e-10
45	1.5708	6.89e-11
50	1.5708	9.29e-11
55	1.5708	9.13e-11
60	1.5708	5.14e-11
65	1.5708	5.08e-11
70	1.5708	1.36e-10
75	1.5708	1.31e-10
80	1.5708	7.47e-11
85	1.5708	1.01e-10
90	1.5708	8.11e-11
95	1.5708	8.49e-11
100	1.5708	1.55e-10

(b) Scaled quadrature

Table B.3: Computations of $I = \int_0^\infty \operatorname{sech}(x)dx$ for different orders.

Order, n	Solution	Error, $\frac{(a-b)}{a}$
5	0.9882	0.0118
10	1.0007	0.000676
15	0.99996	4.22e-05
20	1.0000	4.08e-06
25	1.0000	1.74e-06
30	1.0000	1.25e-08
35	1.0000	8.23e-08
40	1.0000	4.08e-09
45	1.0000	5.22e-09
50	1.0000	1.07e-09
55	1.0000	2.57e-10
60	1.0000	1.72e-10
65	1.0000	2.37e-11
70	1.0000	1.05e-11
75	1.0000	5.14e-12
80	1.0000	4.66e-13
85	1.0000	1.59e-12
90	1.0000	1.05e-12
95	1.0000	4.81e-13
100	1.0000	1.84e-13

(a) Normal quadrature

Order, n	Solution	Error, $\frac{(a-b)}{a}$
5	0.9881	0.0119
10	1.0000	1.16e-06
15	1.0000	1.69e-09
20	1.0000	6.38e-11
25	1.0000	5.16e-11
30	1.0000	3.38e-11
35	1.0000	1.13e-10
40	1.0000	9.85e-11
45	1.0000	6.58e-11
50	1.0000	9.15e-11
55	1.0000	8.33e-11
60	1.0000	4.4e-11
65	1.0000	4.36e-11
70	1.0000	1.27e-10
75	1.0000	1.25e-10
80	1.0000	6.09e-11
85	1.0000	8.47e-11
90	1.0000	6.63e-11
95	1.0000	7.1e-11
100	1.0000	1.39e-10

(b) Scaled quadrature

Table B.4: Computations of $I = \int_0^\infty \operatorname{sech}^2(x)dx$ for different orders.

Order, n	Solution	Error, $\left\lvert\frac{(a-b)}{a}\right\rvert$
5	2.4676	7.82e-05
10	2.4674	1.12e-06
15	2.4674	4.31e-08
20	2.4674	1.86e-09
25	2.4674	5.95e-11
30	2.4674	1.39e-11
35	2.4674	4.48e-11
40	2.4674	2.03e-11
45	2.4674	2.39e-11
50	2.4674	2.47e-11
55	2.4674	1.52e-11
60	2.4674	1.11e-11
65	2.4674	7.7e-12
70	2.4674	5.08e-12
75	2.4674	3.21e-12
80	2.4674	1.94e-12
85	2.4674	1.11e-12
90	2.4674	6.11e-13
95	2.4674	3.14e-13
100	2.4674	1.51e-13

(a) Normal quadrature

Order, n	Solution	Error, $\left\lvert\frac{(a-b)}{a}\right\rvert$
5	2.4456	0.00883
10	2.4674	1.11e-06
15	2.4674	5.63e-11
20	2.4674	7.2e-11
25	2.4674	6.75e-11
30	2.4674	4.04e-11
35	2.4674	1.11e-10
40	2.4674	1.36e-10
45	2.4674	8.6e-11
50	2.4674	1.17e-10
55	2.4674	1.3e-10
60	2.4674	6.96e-11
65	2.4674	6.73e-11
70	2.4674	1.95e-10
75	2.4674	1.84e-10
80	2.4674	1.06e-10
85	2.4674	1.48e-10
90	2.4674	1.15e-10
95	2.4674	1.19e-10
100	2.4674	2.25e-10

(b) Scaled quadrature

Table B.5: Computations of $I = \int_0^\infty x\,\mathrm{csch}(x)dx$ for different orders.

B.3 Integrands Involving Products of Different Types of Functions

In this section, exponential and hyperbolic functions will be multiplied with other functions, then their integrals will be evaluated. First, the integral

$$\int_0^\infty \frac{e^{-x}}{\sqrt{x}} dx, \tag{B.9}$$

will be computed. This is, by definition, equal to the gamma function $\Gamma(z)$ with an argument of $z = 1/2$. The solution is known to be equal to $\sqrt{\pi}$, and it is expected that the computation will give a result close to this value. However, neither the scaled nor the unscaled quadrature provides an accurate result. This is most probably due to the singularity of the integrand at $x = 0$. As can be seen in Table B.6a, there is quite a significant error even when $n = 150$ for the normal quadrature. For the scaled quadrature, the error is less; however, it is still quite significant. Furthermore, the decrease in error is quite slow. In other words, the convergence to the actual result is slow. Even though the integral is singular, this is puzzling at first. Because, analytically, the solution is known, and while the first root of the Laguerre polynomials may be close to $x = 0$, it never is zero. For example, the first root of $L_{150}(x)$ is roughly $9.6 \cdot 10^{-3}$. Even if when the scaling factor was of order $O(10^{-3})$, the value of $1/\sqrt{x}$ would be of order $O(10^5)$. However, the addition and subtraction of relatively small values ($O(10^1)$ or less), with the initially large results, lead to considerable errors. Therefore, this quadrature is not the ideal method to solve this integral.

Next, the integrals

$$\int_0^\infty e^{-x^2} \cos(x) dx \quad \text{and} \quad \int_0^\infty e^{-x^2} \cos(5x) dx, \tag{B.10}$$

are to be computed. Notice that this is equal to the Fourier-cosine transform of e^{-x^2} at specific frequency values ($\omega = 1$ and $\omega = 5$, respectively). The solutions can thus be found using tables of Fourier transforms, such as the table prepared by Oberhettinger (2012). The results of the first integral are given in Table B.7. Both the normal and the scaled quadratures give very accurate results, with the scaled quadrature converging faster, the same as before. As for the second integral, its results are given in Table B.8. As can be seen, the normal quadrature has difficulties computing the integral accurately since the integrand is quite oscillatory and the integral value is quite

small. However, the scaled quadrature performs quite well. Note that the error of the normal quadrature never becomes less than that of the scaled one. The errors do not even compare, showing the difficulty posed by oscillatory integrands.

Now, the integrals

$$\int_0^\infty \operatorname{sech}(x)\cos(x)dx \quad \text{and} \quad \int_0^\infty \operatorname{sech}(x)\cos(5x)dx, \tag{B.11}$$

are going to be computed. Similar to the previous case, the values will be found from Fourier-cosine transform tables. Similar to the last case, for $\cos(x)$ the two forms of the quadrature yield comparable and accurate results, even though the scaled quadrature converges more quickly. However, for $\cos(5x)$ the scaled quadrature yields quite accurate results for higher-order, whereas the normal quadrature does not. In fact, in this case, the normal quadrature yields considerably erroneous results and further shows the difficulty of computing highly oscillatory integrals.

Lastly, the integrals

$$\int_0^\infty \operatorname{sech}^2(x)\cos(x)dx \quad \text{and} \quad \int_0^\infty \operatorname{sech}^2(x)\cos(5x)dx, \tag{B.12}$$

will be computed. Again, the Fourier-cosine tables will be made use of. Clearly, the scaled quadrature performs better, again. However, unlike the integrals of $e^{-x^2}\cos(5x)$ and $\operatorname{sech}(x)\cos(5x)$, the results using larger orders are quite close to each other for the integral of $\operatorname{sech}^2(x)\cos(5x)$. This is quite interesting since it was expected that the normal quadrature would perform badly even for high orders.

Order, n	Solution	Error, $\left\lvert\frac{(a-b)}{a}\right\rvert$
25	1.5992	0.0977
30	1.6142	0.0893
35	1.6258	0.0827
40	1.6352	0.0774
45	1.643	0.073
50	1.6496	0.0693
55	1.6553	0.0661
60	1.6603	0.0633
65	1.6647	0.0608
70	1.6686	0.0586
75	1.6721	0.0566
80	1.6753	0.0548
85	1.6782	0.0532
90	1.6808	0.0517
95	1.6832	0.0503
100	1.6855	0.0491
105	1.6876	0.0479
110	1.6895	0.0468
115	1.6914	0.0458
120	1.6931	0.0448
125	1.6947	0.0439
130	1.6962	0.043
135	1.6976	0.0422
140	1.6989	0.0415
145	1.7002	0.0408
150	1.7014	0.0401

(a) Normal quadrature

Order, n	Solution	Error, $\left\lvert\frac{(a-b)}{a}\right\rvert$
25	1.6889	0.0472
30	1.7033	0.039
35	1.7135	0.0332
40	1.7211	0.029
45	1.727	0.0256
50	1.7317	0.023
55	1.7355	0.0209
60	1.7386	0.0191
65	1.7413	0.0176
70	1.7436	0.0163
75	1.7456	0.0152
80	1.7473	0.0142
85	1.7488	0.0134
90	1.7501	0.0126
95	1.7513	0.0119
100	1.7524	0.0113
105	1.7534	0.0108
110	1.7542	0.0103
115	1.7551	0.00982
120	1.7558	0.0094
125	1.7565	0.00902
130	1.7571	0.00867
135	1.7577	0.00834
140	1.7582	0.00804
145	1.7587	0.00776
150	1.7592	0.00749

(b) Scaled quadrature

Table B.6: Computations of $I = \int_0^\infty e^{-x}/\sqrt{x}dx$ for different orders.

Order, n	Solution	Error, $\frac{(a-b)}{a}$
5	0.64648	0.0633
10	0.69644	0.00905
15	0.68942	0.00112
20	0.69033	0.000198
25	0.69016	4.8e-05
30	0.6902	1.27e-05
35	0.69019	2.99e-06
40	0.69019	4.68e-07
45	0.69019	2.65e-08
50	0.69019	5.01e-08
55	0.69019	1.76e-08
60	0.69019	1.88e-09
65	0.69019	1.06e-09
70	0.69019	5.44e-10
75	0.69019	5.2e-11
80	0.69019	4.7e-11
85	0.69019	1.8e-11
90	0.69019	8.64e-13
95	0.69019	2.85e-12
100	0.69019	1.85e-13

(a) Normal quadrature

Order, n	Solution	Error, $\frac{(a-b)}{a}$
5	0.68697	0.00467
10	0.69019	2.6e-07
15	0.69019	6.04e-11
20	0.69019	7.24e-11
25	0.69019	8.48e-11
30	0.69019	5.57e-11
35	0.69019	1.09e-10
40	0.69019	2.19e-10
45	0.69019	1.38e-10
50	0.69019	1.73e-10
55	0.69019	2.55e-10
60	0.69019	1.5e-10
65	0.69019	1.42e-10
70	0.69019	3.65e-10
75	0.69019	3.22e-10
80	0.69019	2.56e-10
85	0.69019	3.49e-10
90	0.69019	2.77e-10
95	0.69019	2.73e-10
100	0.69019	4.67e-10

(b) Scaled quadrature

Table B.7: Computations of $I = \int_0^\infty e^{-x^2} \cos(x) dx$ for different orders.

Order, n	Solution	Error, $\frac{(a-b)}{a}$
5	0.31598	184
10	-0.20625	122
15	0.07055	40.2
20	-0.0042949	3.51
25	-0.0093535	6.47
30	0.010817	5.32
35	-0.0018028	2.05
40	0.0019047	0.113
45	0.0022925	0.34
50	0.0014131	0.174
55	0.001716	0.00302
60	0.0017683	0.0336
65	0.0016912	0.0114
70	0.0017046	0.00361
75	0.0017165	0.00331
80	0.0017109	2.50e-05
85	0.0017096	0.000715
90	0.001711	0.000115
95	0.0017111	0.000142
100	0.0017107	4.23e-05

(a) Normal quadrature

Order, n	Solution	Error, $\frac{(a-b)}{a}$
5	-0.11772	69.8
10	0.0023903	0.397
15	0.0017112	0.000214
20	0.0017108	7.96e-07
25	0.0017108	6.74e-09
30	0.0017108	1.62e-08
35	0.0017108	4.43e-08
40	0.0017108	2.52e-08
45	0.0017108	2.91e-08
50	0.0017108	3.57e-08
55	0.0017108	1.81e-08
60	0.0017108	4.27e-08
65	0.0017108	5.7e-08
70	0.0017108	4.18e-08
75	0.0017108	6.77e-09
80	0.0017108	1.22e-07
85	0.0017108	7.44e-08
90	0.0017108	1.14e-07
95	0.0017108	1.2e-07
100	0.0017108	2.56e-08

(b) Scaled quadrature

Table B.8: Computations of $I = \int_0^\infty e^{-x^2} \cos(5x)dx$ for different orders.

Order, n	Solution	Error, $\frac{(a-b)}{a}$
5	0.62023	0.00925
10	0.62631	0.000469
15	0.62599	4.51e-05
20	0.62602	2.06e-06
25	0.62602	6.93e-07
30	0.62602	1.12e-07
35	0.62602	2.59e-08
40	0.62602	4.63e-09
45	0.62602	2.00e-09
50	0.62602	4.34e-11
55	0.62602	1.56e-10
60	0.62602	2.84e-11
65	0.62602	9.55e-12
70	0.62602	6.05e-12
75	0.62602	3.36e-13
80	0.62602	1.35e-12
85	0.62602	1.17e-12
90	0.62602	7.43e-13
95	0.62602	4.54e-13
100	0.62602	2.61e-13

(a) Normal quadrature

Order, n	Solution	Error, $\frac{(a-b)}{a}$
5	0.65756	0.0504
10	0.62601	1.48e-05
15	0.62602	1.37e-07
20	0.62602	2.4e-10
25	0.62602	5.32e-11
30	0.62602	8.48e-12
35	0.62602	1.15e-10
40	0.62602	1.45e-10
45	0.62602	5.25e-11
50	0.62602	8.12e-11
55	0.62602	1.62e-10
60	0.62602	6.3e-11
65	0.62602	5.52e-11
70	0.62602	2.56e-10
75	0.62602	2.27e-10
80	0.62602	8.5e-11
85	0.62602	1.5e-10
90	0.62602	9.36e-11
95	0.62602	9.59e-11
100	0.62602	2.62e-10

(b) Scaled quadrature

Table B.9: Computations of $I = \int_0^\infty \operatorname{sech}(x)\cos(x)dx$ for different orders.

Order, n	Solution	Error, $\frac{(a-b)}{a}$
5	0.79092	648
10	-0.74363	611
15	0.45074	369
20	-0.15021	124
25	-0.0037571	4.08
30	0.047116	37.6
35	-0.03446	29.3
40	0.017767	13.6
45	-0.0027699	3.27
50	0.00018225	0.851
55	0.0030343	1.49
60	5.5915e-05	0.954
65	0.0016808	0.378
70	0.0011455	0.0608
75	0.0011648	0.0449
80	0.0012799	0.0495
85	0.0011861	0.0274
90	0.0012309	0.00927
95	0.0012189	0.000574
100	0.0012174	0.00177

(a) Normal quadrature

Order, n	Solution	Error, $\frac{(a-b)}{a}$
5	-1.4716	1210
10	-0.73871	607
15	0.12574	102
20	-0.016771	14.8
25	0.00040652	0.667
30	0.0011808	0.0318
35	0.0012111	0.00692
40	0.0012186	0.000763
45	0.0012195	4.22e-05
50	0.0012196	1.51e-05
55	0.0012196	2.50e-06
60	0.0012196	3.42e-07
65	0.0012196	3.98e-07
70	0.0012196	3.12e-08
75	0.0012196	8.30e-10
80	0.0012196	2.94e-08
85	0.0012196	4.25e-08
90	0.0012196	3.2e-09
95	0.0012196	3.44e-08
100	0.0012196	2.97e-08

(b) Scaled quadrature

Table B.10: Computations of $I = \int_0^\infty \operatorname{sech}(x)\cos(5x)dx$ for different orders.

Order, n	Solution	Error, $\frac{(a-b)}{a}$
5	0.65887	0.0347
10	0.684	0.00209
15	0.68249	0.000117
20	0.68256	1.67e-05
25	0.68257	5.81e-06
30	0.68257	1.4e-07
35	0.68257	2.81e-07
40	0.68257	1.88e-08
45	0.68257	1.75e-08
50	0.68257	4.03e-09
55	0.68257	7.84e-10
60	0.68257	5.87e-10
65	0.68257	7.89e-11
70	0.68257	4.4e-11
75	0.68257	2.54e-11
80	0.68257	3.55e-12
85	0.68257	2.49e-12
90	0.68257	1.93e-12
95	0.68257	7.28e-13
100	0.68257	1.58e-13

(a) Normal quadrature

Order, n	Solution	Error, $\frac{(a-b)}{a}$
5	0.66834	0.0209
10	0.68256	7.23e-06
15	0.68257	6.36e-09
20	0.68257	4.36e-11
25	0.68257	1.7e-11
30	0.68257	1.99e-11
35	0.68257	1.21e-10
40	0.68257	1.09e-11
45	0.68257	2.29e-11
50	0.68257	3.58e-11
55	0.68257	1.98e-11
60	0.68257	6.56e-12
65	0.68257	2.02e-12
70	0.68257	2.68e-11
75	0.68257	7.64e-12
80	0.68257	2.16e-11
85	0.68257	4.05e-11
90	0.68257	2.46e-11
95	0.68257	1.85e-11
100	0.68257	4.41e-11

(b) Scaled quadrature

Table B.11: Computations of $I = \int_0^\infty \operatorname{sech}^2(x)\cos(x)dx$ for different orders.

Order, n	Solution	Error, $\frac{(a-b)}{a}$
5	0.409	66.1
10	-0.30554	51.1
15	0.1461	23
20	-0.041059	7.73
25	0.018867	2.09
30	0.0030757	0.496
35	0.0068383	0.121
40	0.0059081	0.0311
45	0.0061331	0.00578
50	0.0060962	0.000278
55	0.0060971	0.000131
60	0.0060983	7.65e-05
65	0.0060976	5.09e-05
70	0.006098	1.69e-05
75	0.0060979	3.61e-06
80	0.0060979	1.66e-06
85	0.0060979	4.03e-07
90	0.0060979	1.18e-08
95	0.0060979	4.23e-08
100	0.0060979	1.92e-09

(a) Normal quadrature

Order, n	Solution	Error, $\frac{(a-b)}{a}$
5	-0.12554	21.6
10	-0.053102	9.71
15	0.0059509	0.0241
20	0.0060999	0.000325
25	0.0060979	3.80e-06
30	0.0060979	2.27e-07
35	0.0060979	1.81e-08
40	0.0060979	2.65e-09
45	0.0060979	5.13e-09
50	0.0060979	1.3e-08
55	0.0060979	8.86e-09
60	0.0060979	1.43e-09
65	0.0060979	1.81e-09
70	0.0060979	6.46e-09
75	0.0060979	1.38e-09
80	0.0060979	4.64e-09
85	0.0060979	8.92e-09
90	0.0060979	4.16e-09
95	0.0060979	2.35e-09
100	0.0060979	9.58e-09

(b) Scaled quadrature

Table B.12: Computations of $I = \int_0^\infty \operatorname{sech}^2(x)\cos(5x)dx$ for different orders.